Probing the Active Site Residues of a Prephenate Dehydrogenase from the Hyperthermophilic Bacterium *Aquifex aeolicus*

Wenjuan Hou

A Thesis

In

The Department

Of

Biology

Presented in Partial Fulfillment of the Requirements

for the Degree of Master of Science at

Concordia University

Montreal, Quebec, Canada

March 2009

© Wenjuan Hou, 2009

Library and Archives Canada

Published Heritage Branch

395 Wellington Street
Ottawa ON K1A 0N4
Canada

Bibliothèque et Archives Canada

Direction du Patrimoine de l'édition

395, rue Wellington
Ottawa ON K1A 0N4
Canada

Your file Votre référence
ISBN: 978-0-494-63222-2
Our file Notre référence
ISBN: 978-0-494-63222-2

NOTICE:

The author has granted a non-exclusive license allowing Library and Archives Canada to reproduce, publish, archive, preserve, conserve, communicate to the public by telecommunication or on the Internet, loan, distribute and sell theses worldwide, for commercial or non-commercial purposes, in microform, paper, electronic and/or any other formats.

The author retains copyright ownership and moral rights in this thesis. Neither the thesis nor substantial extracts from it may be printed or otherwise reproduced without the author's permission.

AVIS:

L'auteur a accordé une licence non exclusive permettant à la Bibliothèque et Archives Canada de reproduire, publier, archiver, sauvegarder, conserver, transmettre au public par télécommunication ou par l'Internet, prêter, distribuer et vendre des thèses partout dans le monde, à des fins commerciales ou autres, sur support microforme, papier, électronique et/ou autres formats.

L'auteur conserve la propriété du droit d'auteur et des droits moraux qui protège cette thèse. Ni la thèse ni des extraits substantiels de celle-ci ne doivent être imprimés ou autrement reproduits sans son autorisation.

In compliance with the Canadian Privacy Act some supporting forms may have been removed from this thesis.

While these forms may be included in the document page count, their removal does not represent any loss of content from the thesis.

Conformément à la loi canadienne sur la protection de la vie privée, quelques formulaires secondaires ont été enlevés de cette thèse.

Bien que ces formulaires aient inclus dans la pagination, il n'y aura aucun contenu manquant.

Canada

Abstract

Probing the Importance of Active Site Residues of Prephenate Dehydrogenase from the Hyperthermophilic Bacterium *Aquifex aeolicus*

Wenjuan Hou, M.Sc.

Prephenate dehydrogenase is an enzyme within the TyrA protein family dedicated to tyrosine biosynthesis. It catalyzes the oxidative decarboxylation of prephenate to hydroxyphenylpyruvate (HPP) and CO_2 in the presence of NAD^+; HPP is then transaminated to L-tyrosine, an end product inhibitor of the pathway. Guided by the recently published crystal structures of a monofunctional prephenate dehydrogenase from the hyperthermophilic bacterium *Aquifex aeolicus*, amino acid residues Trp190, His217, Lys246' and Arg250 were targeted for mutagenesis in order to provide insights into how these side chains might participate in the chemistry of the reaction and contribute to the integrity of the active site. A revised purification protocol afforded excellent yields of variants. We identified Trp190, a completely buried side chain in the NAD^+ binding pocket, as the source of an unusual fluorescence emission peak at 317 nm. Analysis of variants of Lys246' and Arg250 allowed us to conclude that the two residues participated only in the binding of prephenate and not of NAD^+ or in catalysis. They are important residues but not essential for binding. In contrast, His217 is critical for prephenate binding and catalysis and for the inhibition of PD activity by tyrosine. Chemical and thermal denaturation studies also suggest that this residue helps to maintain the structural integrity of the active site. Our results are interpreted in light of the crystal structure of the enzyme bound with substrate analogues and tyrosine.

Acknowledgements

I would like to thank my thesis supervisor Dr. Joanne Turnbull for her supervision, consultation, support and patience. I also want to thank her for guiding me with the scientific standards. I would like to thank my examining committee members Dr. Paul Joyce and Dr. Vincent Martin, for their suggestions, time and effort during my master studies. I would like to thank Dr. Luc Varin for being my external examiner of my thesis defense. I would like to thank the center for Structural and Functional Genomics and also Alain Tessier for his kind help and the training on the Q-ToF instruments in the Center for Biological Applications of Mass Spectrometry. I would like to thank my formal colleagues Dr. Julie Bonvin and Dr. John Manioudakis for their grateful help and patience along my studies. I also want to thank my other colleagues Said Hassounah, Peter Quashie, Francis McManus, Nicholas Sitaras, Natasha Hotz, Jason Arthor, Biao Shen, Mengwei Ye and Yu Lei for their help and suggestions. A special thanks to my best friend Zhejun Wang and my boyfriend Wentao Fan for being there for me in the good and bad time. Finally, I would like to give a big warm thank you to my family for their love, support and encouragement through the numerous years of studies.

Table of Contents

List of Figures

List of Tables

List of Abbreviations

AD	Arogenate dehydrogenase
ADT	Arogenate dehydratase
Ala (A)	Alanine
Arg (R)	Arginine
Asp (D)	Aspartic acid
bp	Base pair
BSA	Bovine serum albumin
CD	Circular dichroism
CM	Chorismate mutase
CM-PD	Chorismate mutase-prephenate dehydrogenase
Da	Dalton
DEPC	Diethyl pyrocarbonate
DHAP synthetase	3-deoxy-D-arabino-heptulosonic acid-7-phosphate synthetase
DNA	Deoxyribonucleic acid
DTT	Dithiothreitol
EDTA	Ethylenediamine tetra-acetic acid
ESI- Q-ToF	Electrospray ionization Quadrupole Time-of-Flight
Gdn-HCl	Guanidinium hydrochloride
Gln (Q)	Glutamine
Glu (E)	Glutamic acid
HEPES	4-(2-hydroxyethyl)-1-piperazineethanesulfonic acid
His (H)	Histidine
H_2O	Water
HPlactate	4-hydroxyphenyl lactate
HPP	4-hydroxyphenyl pyruvate
HPpropionate	4-hydroxyphenyl propionate
Ile (I)	Isoleucine
IPTG	Isopropyl-β-D-thiogalactopyranoside
k_{cat}	Turnover number
K_i	Inhibition constant

K_m	Michaelis constant
LB	Luria-Bertani broth
Lys (K)	Lysine
MS	Mass spectrometry
MW	Molecular weight
$NAD^+(H)$	Oxidized (reduced) forms of nicotinamide adenine dinucleotide
Ni-NTA	Nickel-nitrilotriacetic acid
PCR	Polymerase chain reaction
PD	Prephenate dehydrogenase
PDT	Prephenate dehydratase
PMSF	Phenylmethylsulfonyl fluoride
PP	Phenylpyruvate
SDS-PAGE	Sodium dodecyl sulfate- polyacrylamide gel electrophoresis
TE	Tris/EDTA
TECP-HCl	Tris (2-carboxyethyl) phosphine hydrochloride
TEMED	N,N,N',N'-tetramethylethylenediamine
Trp (W)	Tryptophan
Tyr (Y)	Tyrosine
U	Units
UV	Ultraviolet
V_{max}	Maximum velocity
VT-FTIR	Variable temperature-fourier transform infrared spectroscopy

Chapter 1: Introduction

1.1 Aromatic Amino Acids Biosynthesis

The aromatic amino acids, L-tyrosine, L-tryptophan, and L-phenylalanine are vital for growth and maintenance of all living organisms. The metabolic pathway for producing these amino acids (Figure 1) is found only in micro-organisms, fungi and plants; animals take in these essential amino acids from their diet (*1*). This pathway, known as the shikimate pathway, links carbohydrate metabolism to the biosynthesis of aromatic compounds. It encompasses seven metabolic steps initiated by the condensation of derivatives of glucose (erythrose-4-phosphate and phosphoenol-pyruvate) to give 3-deoxy-D-*arabino*-heptulosonate 7-phosphate (DAHP). This seven carbon compound is then cyclised to yield shikimate which is then converted to chorismate. Chorismate serves as the key branch point intermediate and the common precursor of aromatic vitamins, folates, quinones, and aromatic amino acids (*2*). Further steps are found within the "common pathway" (Figure 2). Here, chorismate mutase (CM) catalyzes the Claisen rearrangement of chorismate into prephenate. Prephenate then undergoes dehydration and decarboxylation by prephenate dehydratase (PDT) to yield phenylpyruvate (PP), or is oxidatively decarboxylated by prephenate dehydrogenase (PD) in the presence of NAD^+ to 4-hydroxyphenylpyruvate (HPP) and carbon dioxide (*2*). PP and HPP then undergo transamination to yield L-phenylalanine and L-tyrosine, respectively. The end products act as inhibitors of the mutase, dehydrogenase and dehydratase activities. PD, shown in bold (Figure 2), is the focus of this thesis. Since the biosynthesis of tyrosine is critical for the survival of many organisms, PD, as well as other enzymes in the shikimate and

common pathways, serve as potential targets for the design of inhibitors that can act as antimicrobial agents, fungicides, and herbicides (*3*). Additionally, there is considerable interest in the study of PD and other enzymes in this pathway toward a goal of over-producing tyrosine for the synthesis of commercially valuable compounds, such as drugs (e.g. L-dopa) (*4*), melanin (*5*), and biodegradable polymers (*6*). Hence, understanding the catalytic mechanism and regulation of PD by end products will assist in the design of inhibitors and in the production of tyrosine-insensitive bacterial strains for metabolic engineering.

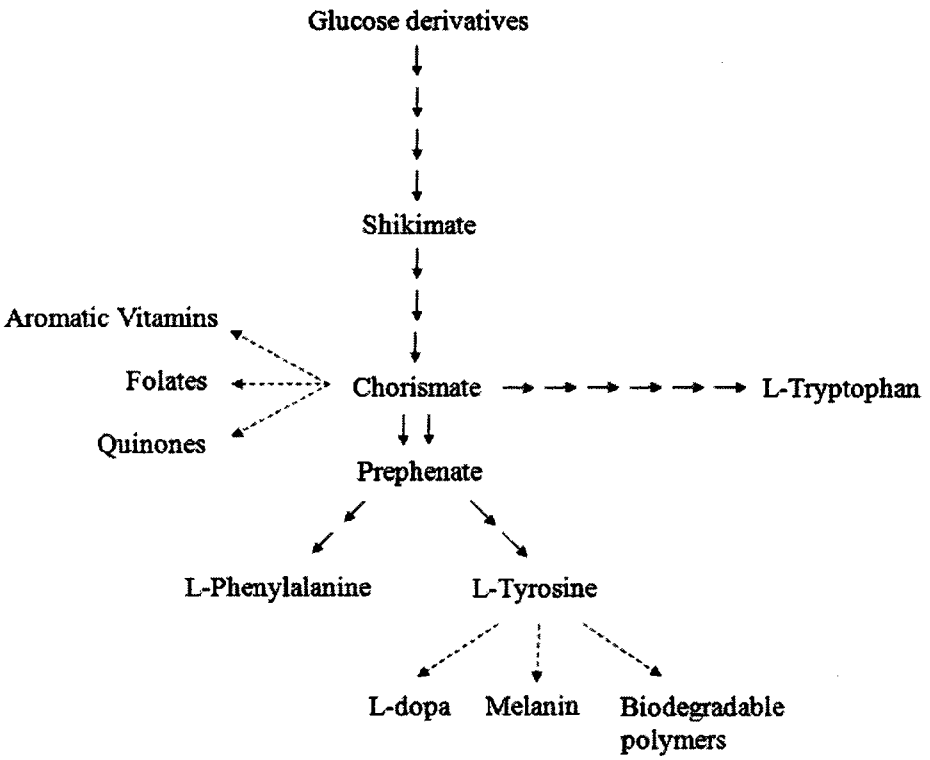

Figure 1: Biosynthetic pathway of aromatic amino acids.

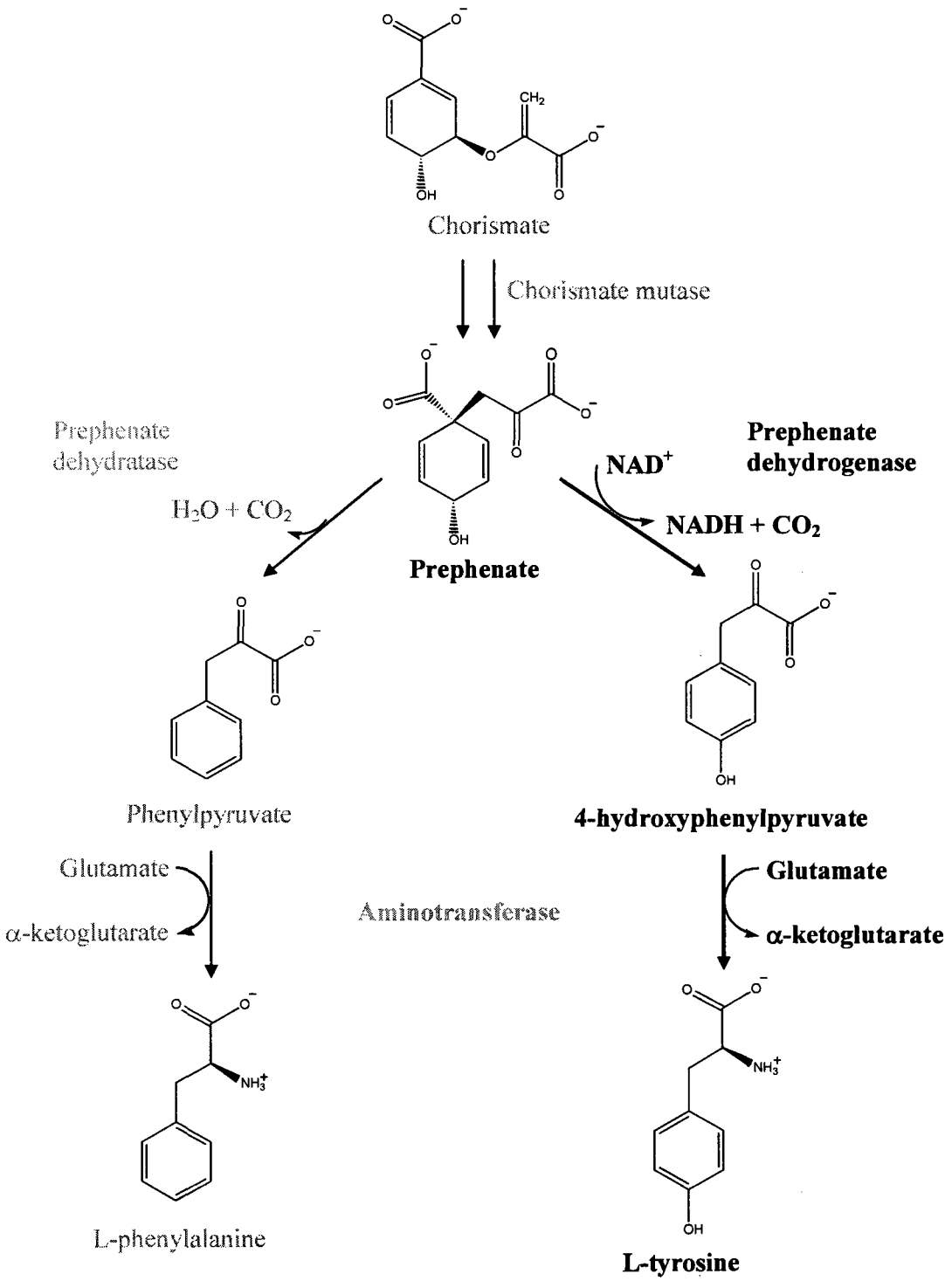

Figure 2: Biosynthesis of L-phenylalanine and L-tyrosine via the "common pathway"

HPP route is in bold.

Many genes encoding the proteins involved in aromatic amino acids biosynthesis are organized in operons. Accordingly, the shikimate pathway is regulated at both the genetic and protein levels. Transcriptional regulators, TyrR, TrpR and PheR, combine with the corresponding co-repressor (tyrosine, tryptophan and phenylalanine) to form a ternary complex at the appropriate operator loci to inhibit transcription. Additional control is also achieved through transcriptional attenuation (premature termination of transcription) at the level of charged tRNA (*7*). However, the major form of regulation is through feedback inhibition of 3-deoxy-D-arabino-heptulosonic acid-7-phosphate synthase (DAHP synthase), CM and PD by the end products of the pathway. DAHP synthase exists in three isoenzyme forms, DAHP Phe, Tyr or Trp, each specific for its appropriate amino acid feedback inhibitor. At the protein level, PD activity has been reported to be regulated by the binding of tyrosine to the active site (*8*), to a distinct allosteric site (*9*) or to a C-terminal domain on the protein (*10*). Accordingly, research efforts are now being directed towards manipulating the regulatory control mechanisms in efforts to increase L-tyrosine production. For example, L-tyrosine overproducing strains of *Corynebacterium glutamicum* and *Escherichia coli* have been generated which contain tyrosine-resistant variants of DAHP synthase and CM-PD (*11, 12*). More recently, an *E. coli* strain has been generated by eliminating the *tyrR* gene combined with over-expressing feedback resistant DAHP synthase and CM-PD proteins in a strain which over-produces the two precursor substrates phosphoenolpyruvate and erythrose-4-phosphate (*13*).

1.2 An Alternative Route to Tyrosine and Phenylalanine Production

As shown in Figure 2, L-tyrosine can be synthesized using HPP as an intermediate. Alternatively, L-tyrosine can be produced by the L-arogenate pathway (Figure 3). Discovered in cyanobacteria by Jensen and coworkers 40 years ago (*14*), prephenate was shown to undergo transamination to yield the cyclohexadienyl amino acid L-arogenate followed by the oxidative decarboxylation of L-arogenate to L-tyrosine, as catalyzed by arogenate dehydrogenase (AD). Similarly, L-phenylalanine can be produced from the PP route catalyzed by PDT or from the reaction of arogenate dehydratase (ADT) which uses L-arogenate (Figure 2 and 3, respectively).

The combination of these two routes (the HPP/PP and the arogenate routes) yields diversity in the biosynthesis of L-tyrosine and L-phenylalanine. In *E. coli* and yeast, tyrosine and phenylalanine are synthesized from HPP and PP, respectively. In most plants however, arogenate is the only pathway for tyrosine and phenylalanine production and is a key branch point for their synthesis. A number of aromatic secondary metabolites derived from L-phenylalanine, such as lignins, hydroxycinnamic amides, flavonoid phytoalexins, are crucial for the survival of plants. Hence, AD is highly sensitive to feedback inhibition by L-tyrosine (*15, 16*); to balance the needs of plant cells, more arogenate is incorporated into the biosynthesis of phenylalanine than tyrosine. In cyanobacteria and some other microrganisms (e.g. *Brevibacterium flavum, B. ammoniagenes* and *Corynebacterium glutamicum*), tyrosine is synthesized via the arogenate pathway while phenylalanine is produced through the PP route (*17-22*).

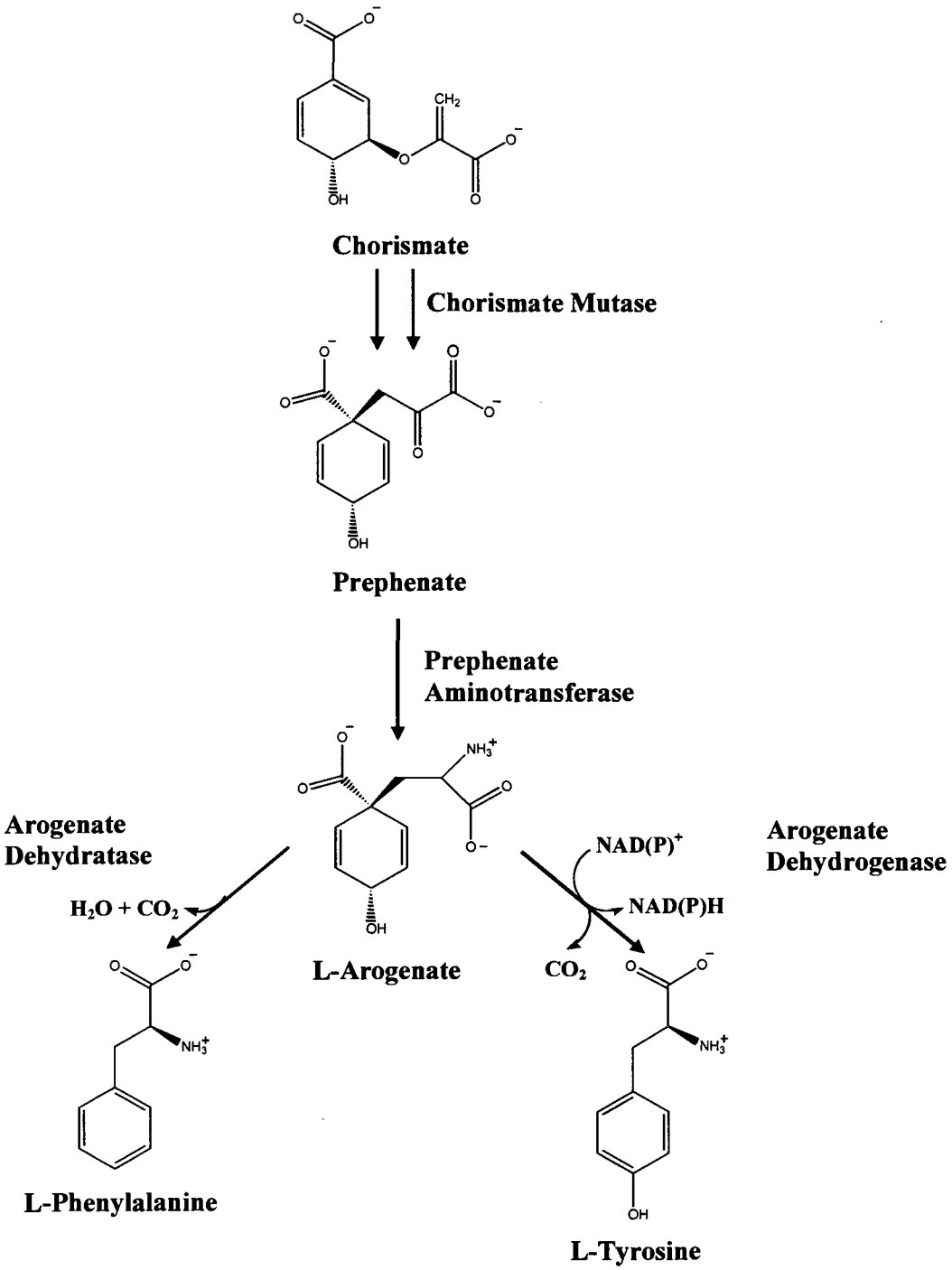

Figure 3: Biosynthesis of L-tyrosine and L-phenylalanine via the arogenate route.

Tyrosine sensitivity is generally associated with TyrA that lie at a key branch point in the biosynthesis of both tyrosine and phenylalanine (*18*). Here, AD is not at the branch point for tyrosine and phenylalanine production; thus this enzyme is insensitive to tyrosine. Additionally, there are other bacterial species, such as *Zymomonas mobilis* (*23*) and *Pseudomonas aeruginosa (24),* that are capable of using both the HPP/PP and arogenate routes to make tyrosine and phenylalanine. *Z. mobilis* TyrA is insensitive to L-tyrosine feedback inhibition while *P. aeruginosa* TyrA (*25*) is inhibited by L-tyrosine.

1.3 The TyrA Protein Family

TyrA proteins encompass a family of dehydrogenases that can be categorized based on their specificities for the cyclohexadienyl substrate (*20, 26*). Prephenate dehydrogenase ($TyrA_p$) and arogenate dehydrogenase ($TyrA_a$) are specific for prephenate and L-arogenate, respectively, while cyclohexadienyl dehydrogenases ($TyrA_c$) can utilize both substrates. Additionally, some dehydrogenases can accept either NAD^+ or $NADP^+$ as cofactors while others can accept both. It is generally noted that prephenate-specific dehydrogenases prefer NAD^+ and arogenate-specific enzymes prefer $NADP^+$ while $TyrA_c$ proteins are capable of utilizing both NAD^+ and $NADP^+$, although they prefer NAD^+ (*26*).

The TyrA family of proteins exists as either monofunctional dehydrogenases or bifunctional enzymes with other activities. For example, PD from *B. subtilis (27)*, AD from *Nicotiana silvestris (28)*, and the cyclohexadienyl dehydrogenase from *Pseudomonas stutzeri (25)* and *Z. mobilis* (*23*) are all monofunctional enzymes. In contrast, PDs from *E. coli* and *Haemophilus influenza* are bifunctional enzymes with CM

activities (*9, 29-31*) and the PDs from *Acinetobacter calcoaceticus* and *Pseudomonas fluorescens* are bifunctional with phosphoskimate carboxyvinyltransferases. Although many proteins within the TyrA family have been tentatively classified according to their substrate specificities and mode of regulation using bioinformatic analysis (see excellent reviews by Jensen and co-workers (*20, 32*)) relatively few enzymes have been cloned, purified and characterized. These include the monofunctional $TyrA_a$ from *Synechocystis sp. (20, 33)*, and $TyrA_c$ *P. stutzeri (25)* and *Z. mobilis (23)* and a bifunctional *E. coli* CM-PD The proposed catalytic mechanism for the dehydrogenase reaction has been established based largely on kinetics and site-directed mutagenesis studies of the *E. coli* CM-PD (*9, 29-31*).

E. coli CM-PD is a homodimer with a molecular weight of ~ 42 kDa per monomer (*8, 34, 35*). Amino acid sequence alignment of *E. coli* CM-PD and CM-PDT, a bifunctional enzyme involved in the biosynthesis of phenylalanine, indicates that the first 100 amino acids of each monomer encode the mutase activity while the remaining 273 residues specify the dehydrogenase activity (*34*). There is kinetic evidence to suggest that the reactions catalyzed by CM and PD occur at distinct active sites (*29, 30, 35-37*); however, their sites may be in close proximity or are inter-related (*29, 36, 38*). No crystallographic data is available for bifunctional CM-PD, although there are structures of related monofuctional CMs bound with the mutase transition-state analogue from a number of organisms, including the independently expressed CM domain of *E. coli* CM-PDT (*39*). Only very recently have there been structures solved for TyrA dehydrogenase proteins. These include the monofunctional PDs from *A. aeolicus (40, 41)* and *H. influenza* (*42*) and AD from *Synechocystis sp.* (*33*).

1.4 Proposed Mechanism for Prephenate Dehydrogenase

A proposed catalytic mechanism for prephenate dehydrogenase (Figure 4) has been established based on isotope effects (*43*), pH rate profiles (*37, 43*), peptide mapping (*29*) and site-directed mutagenesis studies (*30, 31*) of *E. coli* CM-PD. Some of these studies are discussed below.

Prephenate dehydrogenase catalyzes the NAD^+-dependent oxidative decarboxylation of prephenate into 4-hydroxyphenylpyruvate. The reaction is irreversible and driven by the formation of the aromatic product, 4-hydroxyphenylpyruvate. The hydride transfer and decarboxylation steps of the reaction were probed using ^{13}C and deuterium kinetic isotope effect studies. Examination of the rate of C-C cleavage in the decarboxylation step in the presence of deuterated or non-deuterated deoxyprephenate led Hermes *et al.* (*43*) to conclude that hydride transfer and decarboxylation occurred in the same chemical step. The kinetic mechanism of the dehydrogenase reaction of CM-PD has also been investigated. SampathKumar and Morrison (*44*) showed through the analysis of steady-state initial velocity patterns and product and dead-end inhibition studies that PD conforms to random kinetic mechanism with catalysis being the rate-limiting step in the reaction.

Hermes *et al.* (*43*) and Turnbull *et al.* (*37*) showed that a residue with a pK value of 6.5 titrating in the logk_{cat} profile had to be deprotonated for maximum activity. In contrast, the pH dependence of the logk_{cat}/K_m profile displayed, in addition to the deprotonated group, a second ionizing group with a pK value of about 8.4 which was assigned to the binding of prephenate to the enzyme-NAD^+ complex. Further studies by Hermes *et al.* (*43*) on the perturbation of these pK_a groups by temperature and solvent indicated

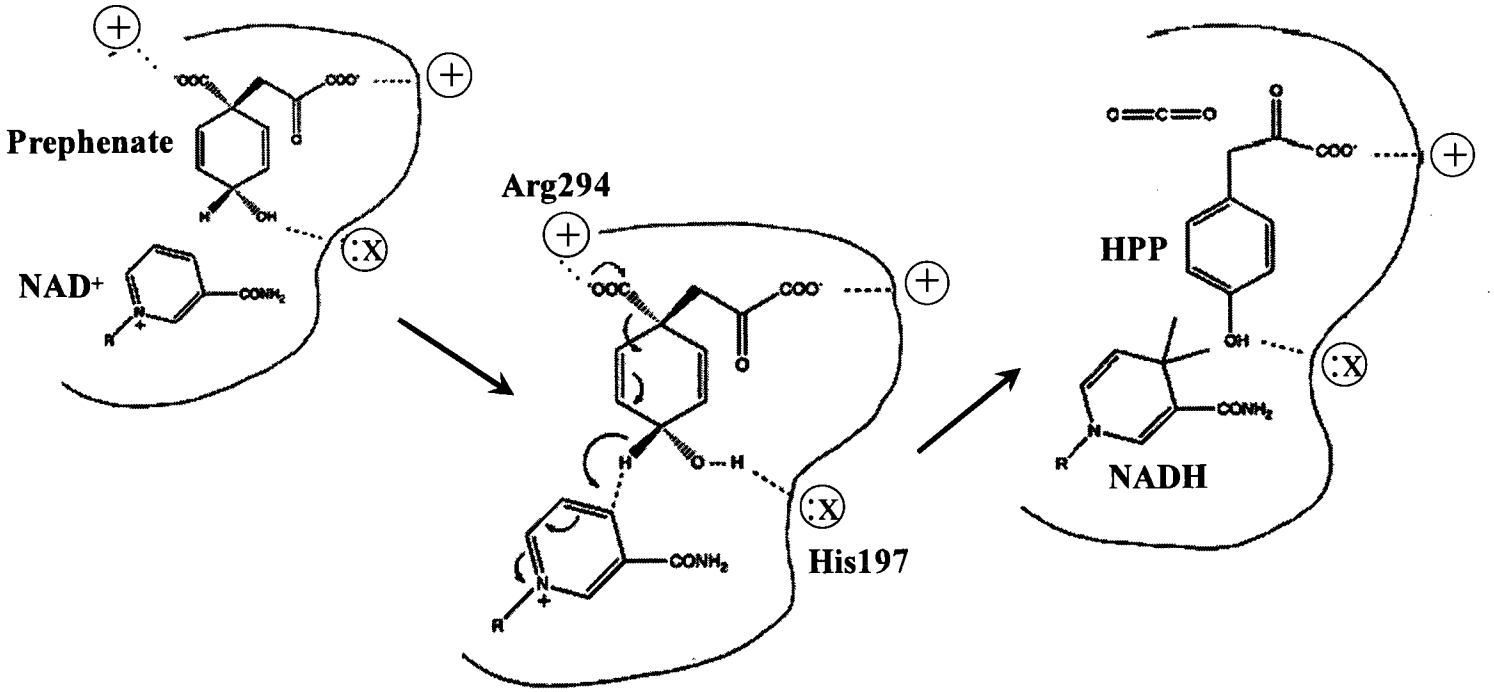

Figure 4: Proposed mechanism for the prephenate dehydrogenase-catalyzed reaction.

Prephenate and NAD^+ bind to different sites at the active site of PD domain. The formation of aromatic product, HPP, provides the driving force to lower the activation energy barrier. His197, a deprotonated group with p*K* value of 6.5 is believed to assist hydride transfer from 4-hydroxyl group of prephenate to NAD^+ and concomitant decarboxylation by polarizing the 4-hydroxyl group. Arg294 was proposed to interact with the ring carboxylate of prephenate bound to the enzyme-NAD^+ complex. In addition, another protonated group with p*K* value of 8.8, is believed to interact with the side chain carboxylate of prephenate to lock prephenate in the active site.

that the catalytic group might be a histidine residue.

Chemical modification of CM-PD with diethyl pyrocarbonate (DEPC) followed by peptide mapping confirmed that a histidine group was near the dehydrogenase active site (*29*). Site-directed mutagenesis studies on CM-PD guided by the analysis of a multiple sequence alignment of several TyrA proteins (see Figure 5) then identified His197 as the critical H-bond acceptor (*30*). The His197Asn variant completely eliminated dehydrogenase activity but had no effect on substrate binding. Moreover, this variant did not alter the mutase activity of the bifunctional enzyme (*30*). The results of site-directed mutagenesis also revealed that a glutamine substitution at Arg294 reduced prephenate binding to the enzyme-NAD^+ complex by 120-fold without affecting the maximum velocity of the dehydrogenase reaction (*31*). It was proposed that Arg294 interacted with the ring carboxylate of prephenate on the basis of the results of inhibition studies with several substrate analogues; compounds that lacked the ring carboxylate group at C-1 position bound with dissociation constants whose values were similar for R294Q and native enzyme. Christendat and Turnbull (*31*) also proposed that a protonated group with a p*K* value of about 8.8 is critical for prephenate binding to the enzyme-NAD^+ complex. However, this group has not yet been identified.

In 2006, Christendat and coworkers (*40*) solved the first crystal structure of a TyrA protein, specifically the hyperthermophilic monofunctional prephenate dehydrogenase from *Aquifex aeolicus* in complex with NAD^+. Prephenate was modeled in the active site. This structure has provided some valuable insights into the position of a number of active site residues. The conserved catalytic group His147 (equivalent to His197 in *E. coli* CM-PD) is located adjacent to the NAD^+ and prephenate to assist in the hydride transfer. The


A.aeolicus ---AILSSMFNPSPPQGFCKKNIIKILKSLSMQNVLIVGVGFMGGSFAKSLRRSGFKGKI 58
H.pylori ----------MKAGIIGLGLMGGSLGLALQEWGRFKSV 28
M.tuberculosis ----------MRAAAAAGREVFGYNRSV 18
Synechocystis ----------MKIGVVGLGLIGASLAGDLRRRG--HYL 26
B.subtilis ----------MNQMKDTILLAGLGLIGGSIALAIKKNHPGKRI 33
S.cerevisiae ----------MVSEDKIEQWKATKVIGIIGLGDMGLLYANKFTDAGWSVIC 41
E.coli ----------VVIVGG-GGQMGRLFEKMLTL 120
H.influenza EKAGISADLIEDVLRRFMRESYANENQFGFKTINSDIHKIVIVGG-YGKLGGLFARYLRA 119
A.aeolicus YGYDINPESISKAVDLGIIDEGTTSIAKVEDFSPDFVMLSSPVRTFREIAKKLSYI-LSE 117
H.pylori TGYDHNALHAKLALTLGLVDECVEFEKILE---CDVIFLAIPVEGIIACLKKMTP--IKK 83
M.tuberculosis EGAHGARSDGFDAIT----DLNQTLTRAAAT--EALIVLAVPMPALPGMLAHIRKS--AP 70
Synechocystis IGVSRQQSTCEKAVERQLVDEAGQDLSLLQT--AKIIFLCTPIQLILPTLEKLIPH-LSP 83
B.subtilis IGIDISDEQAVAALKLGVIDDRADSFISGVK-EAATVIIATPVEQTLVMLEELAHSGIEH 92
S.cerevisiae CDREEYYDELKEKYVSAKFELVKNGHLVSRQ--SDYIIYSVEASNISKIVAMYGPS-SKV 98
E.coli SGYQVRILEQH--------DWDRAADIVAD---AGMVIVSVPIHVTEQVIGKLPP--LPK 167
H.influenza SGYPISILDRE--------DWAVAESILAN---ADVVIVSVPINLTLETIERLKPY-LTE 167
A.aeolicus DATVTDQGSVKGKLVYDLENILGK--RFVGGHPIAGTEKSGVEYSLDNLYEGKKVILTPT 175
H.pylori SATIIDLGGAKAQIIHNIPKSIRK--NFIAAHPMCGTEFYGPKASVKGLYENALVILCDL 141
M.tuberculosis GCPLTDVTSVKCAVLDEVTAAGLQ-ARYVGGHPMTGTAHSGWTAGHGGLFNRAPWVVSVD 129
Synechocystis TAIVTDVASVKTAIAEPASQLWSG---FIGGHPMAGTAAQGIDGAEENLFVNAPYVLTPT 140
B.subtilis ELLITDVGSTKQKVVDYADQVLPSRYQFVGGHPMAGSHKSGVAAAKEFLFENAFYILTPG 152
S.cerevisiae GTIVGGQTSCKLPEIEAFEKYLPKDCDIITVHSLHGPKVN---------TEGQPLVIINH 149
E.coli DCILVDLASVKNGPLQAMLVAHDG--PVLGLHPMFGPDS--------GSLAKQVVVWCDG 217
H.influenza NMLLADLTSVKREPLAKMLEVHSG--AVLGLHPMFGADI--------ASMAKQVVVRCDG 217
A.aeolicus KKTDKKRLKLVKRVWEDVGGVVEYMSPELHDYVFGVVSHLPHAVAFALVDTLIHMS--TP 233
H.pylori EDSGTEQVEIAKEIFLGIKARLIKMKSNEHDTHVAYISHLPHVLSYALANSVLKQ---ND 198
M.tuberculosis DHVDPTVWSMVMTLALDCGAMVVPAKSDEHDAAAAAVSHLPHLLAEALAVTAAEVP---- 185
Synechocystis EYTDPEQLACLRSVLEPLGVKIYLCTPADHDQAVAWISHLPVMVSAALIQACAGEKDGDI 200
B.subtilis QKTDKQAVEQLKNLLKGTNAHFVEMSPEEHDGVTSVISHFPHIVAASLVHQTHHSE--NL 210
S.cerevisiae RSQYPESFEFVNSVMACLKSKQVYLTYEEHDKITADTQAVTHAAFLSMGSAWAKIKIYPW 209
E.coli RKP--EAYQWFLEQIQVWGARLHRISAVEHDQNMAFIQALRHFATFAYGLHLAEEN--VQ 273
H.influenza RFP--ERYEWLLEQIQIWGAKIYQTNATEHDHNMTYIQALRHFSTFANGLHLSKQP--IN 273

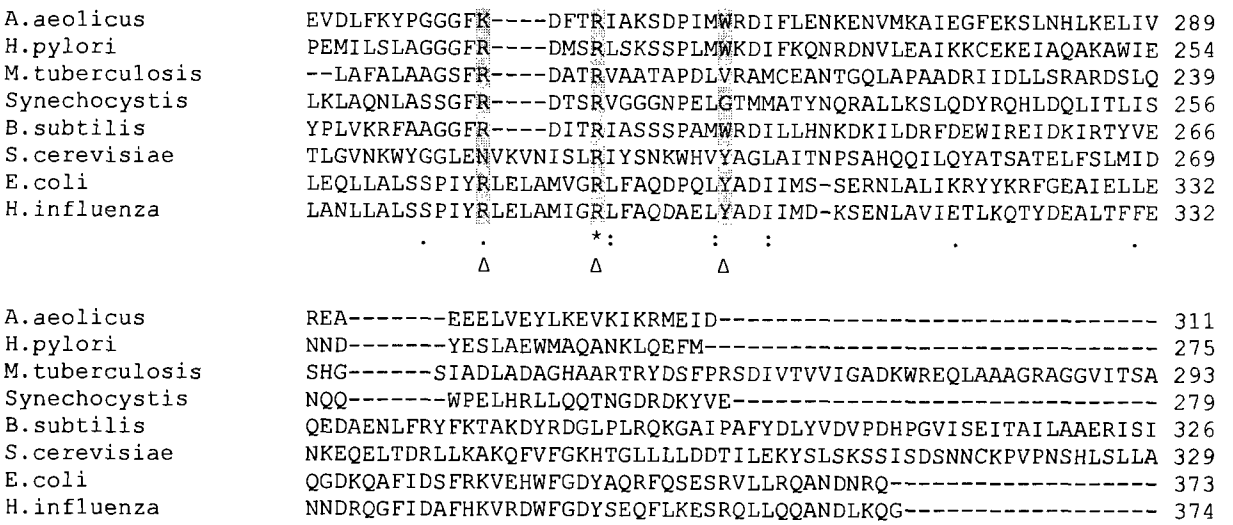

Figure 5: Multiple sequence alignment of PD domains of TyrA proteins

It includes monofunctional PDs from *Aquifex aeolicus*, *Mycobacterium tuberculosis*, *Synechocystis sp.*, *Bacillus subtilis*, *Saccharomyces cerevisiae* and *Helicobacter pylori* and bifunctional CM-PDs from *Escherichia coli* and *Haemophilus influenza*. Conserved residues are highlighted and indicated by an asterisk. Residues studied in the thesis are also highlighted and indicated by a triangle. The catalytic H-bond acceptor is highlighted and indicated by a circle. The multiple sequence alignment was performed using ClustalW2.

conserved Arg250 group involved in substrate binding (equivalent to Arg294 in the *E. coli* enzyme), is in a highly polar environment in close proximity to both the ring carboxylate and the pyruvyl side chain of prephenate and in agreement with the proposed mechanism for PD.

1.5 L-Tyrosine Feedback Inhibition in *E. coli* CM-PD

L-tyrosine, one end product of the aromatic amino acids biosynthesis pathway, serves as an important feedback inhibitor of both the dehydrogenase and mutase activities of *E. coli* CM-PD. The fit of inhibition data to kinetic models combined with the observation that DL-arogenate does not act as a substrate for the *E. coli* PD-catalyzed reaction prompted Turnbull *et al.* (*9*) to conclude that tyrosine binds at an allosteric site. Kinetic studies by others however, suggested that tyrosine and HPP likely compete with each other for binding to the prephenate binding site (*45*). In the *E. coli* enzyme it is well documented that tyrosine binds cooperatively to each of the subunits and enhances the cooperative binding of prephenate (*8*). Analytical ultracentrifugation studies have indicated that the enzyme is able to convert from a dimer to a tetramer in the presence of NAD^+ and tyrosine; it is thought that the dimer is active but the tetramer is inactive, and the presence of NAD^+ promotes the binding of tyrosine to the enzyme and *vice-versa* (*8*). Until recently, residues involved in tyrosine binding were unknown. Stephanopoulos and Lüktke-Eversloh (*12*) identified two residues within the C-terminal region of the *E. coli* CM-PD that are responsible for tyrosine inhibition. Some work will be presented in this thesis on *A. aeolicus* PD which describe the involvement of active site residues in tyrosine binding and inhibition.

1.6 Arogenate Dehydrogenase

As mentioned previously, arogenate dehydrogenase is a member of the TyrA protein family that is dedicated to the biosynthesis of L-tyrosine and L-phenylalanine through the arogenate route in plants, cyanobacteria, and several other microorganisms. Prephenate is first converted to L-arogenate by prephenate transaminase followed by the oxidative decarboxylation of arogenate to tyrosine catalyzed by arogenate dehydrogenase (AD). Legrand *et al. (33)* have recently reported the results of biochemical and crystallographic studies on arogenate dehydrogenase from *Synechocystis* sp.. The work by Legrand and coworkers represents the second reported structure on a TyrA protein; the first structure solved was that of PD from *A. aeolicus* (discussed in section 1.7). They found that this AD strictly uses arogenate and $NADP^+$ as substrates. The enzyme appears to exhibit cooperativity in the binding of arogenate and is insensitive to feedback inhibition by L-tyrosine. Importantly, the crystal structure of the enzyme was solved in complex with $NADP^+$ at pH 8.0 and with L-arogenate modeled in the active site. The overall structure of *Synechocystis* sp. AD is similar to that of *A. aeolicus* PD (Figure 6); both are homodimeric with each monomer encompassing an N-terminal nucleotide binding domain and a C-terminal dimerization domain. The catalytic histidine group (His112) is also conserved in *Synechocystis* sp. AD, (equivalent to His197 in *E. coli* CM-PD and His147 in *A. aeolicus* PD). However, Arg217 in *Synechocystis* sp. AD (equivalent to Arg294 in *E. coli* CM-PD and Arg250 in *A. aeolicus* PD) is reported to be too far from the active site to be involved in substrate binding. The crystal structure of *Synechocystis* sp. AD also revealed that a group of basic residues including Arg213 (equivalent to Lys246' in *A. aeolicus* PD) are located at the interface of the two

monomers and could be involved in electrostatically guiding arogenate to the active site. Additionally, His179, Gly219, Gly221, Gly226, Met228 and Tyr232 were been proposed to be involved in substrate selectivity.

Figure 6: Crystal structure of dimeric *A. aeolicus* Δ19PD complexed with NAD^+ with prephenate modeled in the active site at pH 3.2

One monomer is shown in green and the other one is shown in red. N-terminal domains (lime green and salmon) contain a NAD^+ binding motif; C-terminal domains (green and red) denote dimerization domains. NAD^+ is shown in yellow and modeled prephenate is shown in blue. This picture was created using PyMOL (*46*) and the coordinates derived from ref (*40*).

1.7 *Aquifex aeolicus* Prephenate Dehydrogenase

Aquifex aeolicus is a hyperthermophilic, microaerophilic, obligately chemolithoautotrophic, hydrogen-oxidizing bacterium that can thrive at temperatures greater than 85°C by utilizing hydrogen, carbon dioxide, oxygen and mineral salts (*47, 48*). It cannot grow on organic substrates, such as sugars, amino acids, yeast extract or meat extract. *A. aeolicus* was isolated from the thermal vents of Yellowstone National Park and its entire genomic sequence was reported in 1998 by Deckert *et al* (*49*). A putative *tyrA* gene encoding 311 residues was identified as a PD based on the nucleotide sequence identity to known proteins in GenBank database. The *pheA* gene encoding CM-PDT are found in the genome of *A. aeolicus* (*49*), however, no gene encoding a monofunctional CM was identified. Sequence alignment (Figure 5) shows only 18% amino acid sequence identity between *A. aeolicus* PD and the PD domain of *E. coli* CM-PD but many proposed catalytic and binding groups involved in the PD catalyzed reaction are conserved (*50*).

Efforts to obtain a three-dimensional structure of any TyrA have been largely unsuccessful. In 2006 however, success was achieved with an N-terminally truncated variant of PD from *A. aeolicus*, Δ19PD. The full-length protein did not yield crystals with good diffraction quality. The structure of Δ19PD was solved in complex with NAD^+ although at pH 3.2, likely an inactive form of the enzyme. Δ19PD is a homodimer of 66kDa with 292 amino acids per monomer (*40*). Figure 6 shows that the N-terminal domain of each monomer contains an α/β NAD^+ binding motif while the C-terminal dimerization domain is exclusively α helical (*40*). The active site of PD (one per

monomer) is at the inter-domain cleft of the C-terminal and N-terminal domains (*40*). Residues from each monomer are needed to form the shared active site (*40*).

Concurrently with crystallographic studies Bonvin and coworkers reported the biochemical and biophysical characterization of both the full-length and nd Δ19PD proteins. Both forms were dimeric and showed maximum activity of 95°C or greater and were very resistant to temperature-induced unfolding. PD and Δ19PD were equally effective catalysts, although the k_{cat} and K_m values for prephenate for Δ19PD were twice that of PD. Tyrosine serves as an effective feedback resistant inhibitor of PD activity over a wide temperature range and enhances the cooperativity between substrate in the binding of prephenate. The inhibition by tyrosine did not accompany the formation of a tetramer as reported for *E. coli* CM-PD however (*8, 9, 45*). Low concentrations of guanidine-HCl (Gdn-HCl) activate enzyme activity, but at higher concentrations activity is lost concomitant with a multi-state pathway of denaturation that appears to proceed through oligomerization then to unfolded monomers. Measurements of steady-state fluorescence intensity and its quenching by acrylamide in the presence of Gdn-HCl suggest that, of the two tryptophan residues per monomer, one is buried in a hydrophobic pocket and does not become solvent exposed until the protein unfolds, while the less buried tryptophan is at the active site. Additionally, changes in tryptophan fluorescence emission upon substrate binding revealed that either prephenate or NAD^+ can interact with the unliganded enzyme.

As previously mentioned, the conserved catalytic residue His197 in *E. coli* CM-PD corresponds to His147 in *A. aeolicus* PD while Arg294, the conserved group important for substrate binding in *E. coli* CM-PD is equivalent to Arg250 in *A. aeolicus* PD. The

crystal structure solved at pH 3.2 (*40*) (Figure 7) shows the interaction of key active site groups with prephenate modeled in the active site. His147, the catalytic group, coordinates with the C-4 hydroxyl group of prephenate. The main chain of Ser126 hydrogen bonds to the C-2 hydroxyl group of nicotamide ribose of NAD^+ and may assist in orienting the ring for hydride transfer. His217 may hydrogen bond to the keto-group of the pyruvyl side chain of prephenate. Lys246' from the adjacent monomer is shown to interact with the ring carboxylate group of prephenate when this substrate is modeled in the active site and the guanidinium group of Arg250 is within 4 Å of the ring and side chain carboxylate groups of prephenate. The imidazole ring of His217 participates in hydrophobic stacking with Trp259 (*40*). Additionally, the access of substrate to the active site is believed to be regulated via a gated mechanism which involves an ionic network that consists of Glu153-Arg250-Asp247'(*40, 41*). The importance of some of these residues in this ionic network as well as that of His147 and Ser126 were addressed by preliminary site-directed mutagenesis studies by Bonvin (*51*). We now have structures of Δ19PD bound with NAD^+ and the product HPP as well as L-tyrosine at pH 7.5 (*41*). The interactions will be discussed in light of our results.

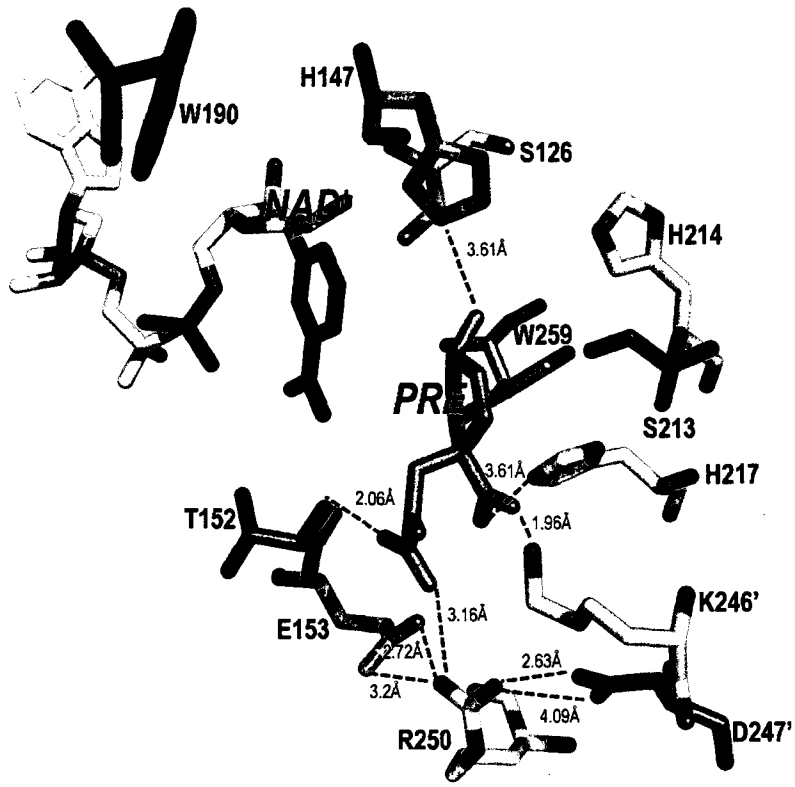

Figure 7: Selected active site residues of *A. aeolicus* Δ19PD complexed with NAD^+ at pH 3.2 and prephenate modeled in the active site

This picture was created using PyMOL (*46*) using the coordinates derived from reference (*40*). The primed residues denoted those groups associated with the adjacent monomer.

1.8 Research Objective

The main goal of this project is to help identify roles of His217, Lys246' and Arg250 residues in the reaction catalyzed by *A. aeolicus* Δ19PD. According to the crystal structure of *A. aeolicus* Δ19PD solved at pH 3.2 (Figure 10) (*40*), His217 may hydrogen bond to the keto-group of the pyruvyl side chain of prephenate and its imidazole ring participates in hydrophobic stacking with Trp259; also, Lys246' might interact with ring carboxylate group of prephenate. Based on the results of kinetics and site-directed mutagenesis studies of *E. coli* CM-PD (*9, 29-31*), Arg294 is believed to be the key group involved in binding prephenate to the enzyme-NAD^+ complex. The sequence alignment between *A. aeolicus* PD and PD domain of *E. coli* CM-PD (Figure 5) shows that Arg294 in *E. coli* CM-PD is equivalent to Arg250 in *A. aeolicus* PD. Therefore, it is important to determine the role of His217, Lys246 and Arg250 involved in reaction catalyzed by PD in solution.

To achieve our goals, the crystal structures of *A. aeolicus* Δ19PD solved at pH 3.2 (*40*) and now very recently at pH 7.5 (*41*) have been used as a guide to select the following variant proteins for study: Trp190Phe, His217Ala, Lys246Ala, Lys246Gln, Arg250Gln, Arg250Ala and Arg250Lys. The *A. aeolicus* Δ19PD variants were generated by site-directed mutagenesis, verified by DNA sequencing, expressed in *E. coli* cells and purified to homogeneity using Ni-NTA affinity chromatography with an improved expression and purification scheme. Then, circular dichroism (CD) and fluorescence spectroscopies were used to examine the secondary and tertiary structures of all variant proteins in comparison to native Δ19PD, and to assess the thermal and chemical stabilities of selected enzymes. Kinetic parameters of these Δ19PD variant proteins were

determined and the results were compared to the native protein. Finally, the effect of L-tyrosine feedback inhibition was examined. Our results are primarily interpreted in light of the crystal structure of *A. aeolicus* Δ19PD complexed with NAD^+ and HPP or NAD^+ plus L-tyrosine.

Part of these findings are now published on-line in the Journal of Biological Chemistry at the following site, http://www.jbc.org/cgi/doi/10.1074/jbc.M806272200, Sun, W., Shahinas, D., Bonvin, J., Hou, W., Kimber, M. S., Turnbull, J. L. and Christendat, D. "The Crystal Structure of *A. aeolicus* Prephenate Dehydrogenase Reveals the Mode of Tyrosine Inhibition".

Chapter 2: Materials and Methods

2.1 Materials

Prephenate (barium salt) was prepared as previously described by Dudzinski and Morrison (*52*) from chorismate, while chorismate (free acid form) was isolated and purified from *Klebsiella pneumonia* (*53*). NAD^+ (grade I) was obtained from Roche. Stock solutions of these substrates were prepared in an appropriate buffer and the pH was adjusted to 7.0 before storage at -20°C. Their exact concentrations were determined using published extinction coefficients (*54*) and enzymatic end-point analysis (*55*). L-tyrosine was purchased from ICN Biochemicals Inc., while *m*-fluoro-DL-tyrosine was purchased from Sigma. Guanidine-HCl (Biotechnology grade), ampicillin (sodium salt), kanamycin sulphate and chloramphenicol were obtained from BioShop and IPTG was from Sigma. HPLC-purified oligonucleotides were from BioCorp (Montreal, QC) while *Dpn*I, *Nde*I, *Bam*HI (all at 10 U/μl), recombinant *Pfu* DNA polymerase (2.5 U/μl) and the deoxy-NTP (dNTP) mixture (5 mM of each dNTP) were purchased from MBI Fermentas. The dNTPs were stored at -20°C in small aliquots. Overnight Express Instant™ TB Medium, BugBuster Protein Extraction reagent and Benzonase Nuclease were from Novagen. Complete™, Mini, EDTA-free protease inhibitor cocktail tablets were purchased from Roche. Phenyl-methyl-sulfonyl fluoride (PMSF) was from EMD Biosciences Inc. and was made up in methanol at 0.5 M and stored at -20°C in 200 μL aliquots. Thrombin protease (purified from bovine plasma, 500 U resuspended in 500 μL of phosphate buffered saline) and NAP™-5 size exclusion buffer exchange columns prepacked with DNA grade Sephadex™ G-25 were purchased from Amersham Biosciences while Ni-

NTA Superflow chromatography resin was supplied by Qiagen. Dialysis membrane (MW cut-off 12-14 kDa) from Spectrapor was washed according to manufacturer's instructions. Ultra free filter units (MW cut-off 10 kDa) were obtained from Amicon. All other chemical reagents and solvents were purchased commercially and were of the highest quality available.

2.2 Strains and Plasmids

The *E. coli* strain XL10-Gold ultracompetent (Stratagene) $Tet^r\Delta$ (*mcrA*)*183* *Δ(marCB-hsdSMR-mrr)173 endA1 supE44 thi-1 recA1 gyrA96 relA1 lac* Hte [F'*proAB* $lacI^qZ\Delta M15$ Tn10 (Tet^r) Amy Cam^r] was used for plasmid production while BL21(DE3) Gold (Stratagene) [F^- dcm^+ Hte ompT hsdS(r_B^- m_B^-) gal λ (DE3) endA Tet^r] and BL21(DE3)pLysS (Promega) [F^-, ompT, $hsdS_B$ (r_B-., m_B-), dcm, gal, λ(DE3), pLysS, Cm^r] were used for protein expression. If not purchased commercially ready to use, cells were rendered competent using calcium chloride (*56*). The helper plasmid pMagik which encodes three rare tRNAs (AGG and AGA for Arg and ATA for Ile) was kindly donated by Dr. A. Edwards, Ontario Cancer Institute, University of Toronto. Recombinant wild-type Δ19PD plasmid was previously constructed by Dr. D. Christendat by cloning *A. aeolicus tyrA* encoding amino acid residues 20-311 of PD into *E. coli* expression vector pET15b (Novagen) which carries a cleavable N-terminal hexahistidine tag (*50*).

2.3 Bacterial Growth Media

LB medium was prepared with 1% tryptone, 0.5% yeast extract and 1% NaCl in distilled H_2O, and the pH was adjusted to 7.5. LB agar was prepared with 1.5% agar in LB medium. NZY^+ broth was prepared with 1% NZ amine (casein hydrolysate), 0.5% yeast extract and 0.5% NaCl in distilled H_2O and the pH was adjusted to 7.5. The media were sterilized by autoclaving at 121°C. Filter-sterilized solutions of 12.5 mM $MgCl_2$, 12.5 mM $MgSO_4$ and 2 % of 20% (w/v) glucose stock were added to the autoclaved NZY^+ broth prior to use. Overnight Express™ Instant TB Medium (30 g) was dissolved in 0.5 L of distilled H_2O supplemented with 5 mL of glycerol. The solution was heated by microwaving for ~ 3 min until bubbles appeared then heated further for another 20 s. Stock solutions of ampicillin (100 mg/mL) and kanamycin (10 mg/mL) were prepared in MilliQ H_2O, filter sterilized by passage through a 0.45 μm syringe (VWR) and then stored at -20°C. Chloramphenicol (34 mg/mL) was prepared in ethanol.

2.4 Site-Directed Mutagenesis

Oligonucleotides were resuspended in 200 μL of MilliQ H_2O and their concentrations were determined from their absorbance at 260 nm. Recombinant *A. aeolicus* Δ19PD plasmid DNA (template) was prepared in TE buffer (10 mM Tris-Cl, 1 mM EDTA, pH 7.4) using PureYield™ Plasmid Maxiprep System (Promega) and deemed free of RNA contamination by agarose gel electrophoresis (section 2.6). Site-directed mutagenesis was conducted using the QuikChange™ method (Stratagene). Each reaction mixture contained double-stranded (ds) template DNA, 125 ng of each oligonucleotide primer (see Table 1), 2 μL of 5 mM dNTP solution, 3 μL of

QuikSolution and 5 μL of 10 x reaction buffer (supplied by the manufacturer) in a final volume of 50 μL. *Pfu* DNA polymerase (2.5-3.75 U/reaction) was added just before the first denaturation cycle. Table 2 lists the amounts of template DNA and *Pfu* DNA polymerase used in the reactions to obtain the mutant plasmids. The primers were extended according to the temperature cycling parameters listed in Table 3. Briefly, dsDNA was denatured at 95°C, oligonucleotide primers were annealed to the denatured DNA template at 60°C, while the synthesis and extension of the new DNA strand complementary to the DNA template was performed at 68°C.

Table 1: Primer sequences for site-directed mutagenesis of *A. aeolicus* Δ19PD

Δ19PD Variants	Oligonucleotide Primer Sequence
W190F	5' TTAAAACTCGTAAAAAGGGTTT**TT**GAAGATGTTGGT 3'
W259F	5' GAGCGACCCCATTATGT**TT**AGAGACATATTTCTGG 3'
R250Q	5' GTTTTAAGGACTTCACG**CA**GATTGCAAAGAGCGACC 3'
R250A	5' GGTTTTAAGGACTTCACG**GC**GATTGCAAAGAGCGAC 3'
R250K	5' GTTTTAAGGACTTCACGA**AA**ATTGCAAAGAGCGACCCC 3'
K246Q	5' CCCGGAGGAGGTTTT**C**AGGACTTCACGAGGATTG 3'
K246A	5' CCCGGAGGAGGTTTT**GC**GGACTTCACGAGGATTG 3'

Primers were designed considering length, GC content and location, and the melting temperature using Primer3 Output program (http://frodo.wi.mit.edu/primer3/input.htm (*57*)). The melting temperature was also verified using the formula in the manual provided by Stratagene. Bold and underlined letters are the bases that were changed from the wild-type sequence. The complementary strands are not shown.

Table 2: Amounts of template DNA and *Pfu* DNA polymerase used in the PCR reaction

Δ19PD Variants	Template DNA (ng)	*Pfu* DNA polymerase (U)
W190F	10	2.5
W259F	10	2.5
K246Q	10	2.5
R250A	20	2.5
R250Q	30	3.75
R250K	30	3.75
K246A	30	3.75

Table 3: Temperature cycling parameters for PCR

Number of Cycles	Temperature (°C)		Time
1	Denaturation	95	1 min
18	Denaturation	95	50 s
	Annealing	60	50 s
	Extension	68	14 min
1	Extension	68	16 min
	Cooling	4	overnight

Upon completion of the temperature cycling, methylated and hemi-methylated parental DNA was digested by incubating 50 μL of the PCR reaction with 10 U of *Dpn*I at 37°C for 100 min. The presence of amplified DNA was confirmed by electrophoresis on a 0.8 % agarose gel (see section 2.6). Digested products were transformed into *E. coli* stain XL10-Gold ultracompetent cells (see section 2.5), and then 500 μL of the culture were plated on LB/agar containing ampicillin (100 μg/mL). A few single colonies derived from overnight growth were selected and inoculated separately into 3-8 mL of liquid LB medium containing ampicillin and grown overnight at 37°C. The plasmid DNA was extracted and purified using the Wizard Plus Miniprep DNA Purification Kit

(Promega). The concentration and purity of plasmid DNA was determined by OD_{260} and OD_{260}/OD_{280}, respectively. The size of plasmid DNA was verified by *Nde*I digestion of the DNA at 37°C for 2 h followed by agarose gel electrophoresis. Generally, the mini-preparations supplied sufficient plasmid DNA for sequencing and for generating stocks for protein expression. If large scale preparations of mutant plasmid DNA were required, plasmid DNA isolated from the mini-preparation was re-transformed into XL10-Gold cells, plated on LB/agar plus ampicillin, and a single colony was used to serially inoculate a 5 mL and then a 100 mL culture. The plasmid DNA from this larger culture was extracted and purified using PureYield™ Plasmid Maxiprep System (Promega) according to the manufacture's instruction and stored in TE buffer at -20°C. Purified DNA was double digested with *Nde*I and *Bam*HI at 37°C for 1 h followed by electrophoretic analysis on a 0.8 % agarose gel in order to verify the size of the insert generated by mutagenesis. An aliquot of undigested plasmid DNA was sent to Bio S&T for sequencing of the *tyrA* gene. The resulting sequences were aligned with that of the wild-type *tyrA* gene, using the BLAST tool in NCBI (http://www.ncbi.nlm.nih.gov/blast/bl2seq/wblast2.cgi) to ensure the desired mutation was achieved and no other mutations had been introduced.

2.5 Transformation

Transformation of *Dpn*I-treated PCR products was carried out according to the protocol outlined in the mutagenesis kit. Briefly, 45 μL of XL10-Gold ultracompetent cells were mixed with 2 μL of β-mercaptoethanol (both supplied by the kit) and incubated on ice for 10 min with periodic gentle swirling. *Dpn*I-treated products (2 μL)

were added to the cell mixture, which were then incubated on ice for 30 min followed by a 30 s heat-shock at 42°C and 2 min incubation on ice. NZY^+ broth (500 μL) was then added to each mixture followed with 1 h shaking (225 rpm) at 37°C. A 500 μL aliquot of the culture was then plated on LB/agar containing 100 μg/mL of ampicillin and grown overnight at 37°C. Alternately, 100 μL of the XL10-Gold cells rendered competent using calcium chloride were directly incubated with 2 μL of *Dpn*I-treated PCR products and the transformations were continued as described above.

Transformation for Δ19PD protein expression was performed based on the method described by Sambrook and Russell *(56)*. Plasmid DNAs (50-100 ng) were mixed with 100 μL of competent cells and incubated on ice for 30 min followed by heat shock for 45 s at 42°C. A further 100 μL of LB was added and the mixture was then incubated at 37°C for 1 h in a water bath. A 200 μL aliquot of the culture was plated on LB/agar containing the appropriate antibiotics and then grown overnight at 37°C.

2.6 Agarose Gel Electrophoresis

Agarose gel electrophoresis (0.8% agarose) was used to assess the size and purity of DNA. Agarose was dissolved to 0.5 x TBE buffer (45 mM Tris-borate/1 mM EDTA, pH ~ 8.3) by heating for 2 min in a microwave. Ethidium bromide (0.5 μg/mL) was then added after the agarose solution had cooled down to 55°C. DNA samples and molecular weight marker (Gene Ruler 1kbp DNA ladder, Fermentas) were mixed with 6 x loading dye (Fermentas). Electrophoresis was performed at 100V until the loading dye migrated to the end of gel (10 cm). DNA was visualized using a UV-transilluminator.

2.7 Expression and Purification of Δ19PD Proteins

Recombinant Δ19PD proteins were expressed and initially purified using a protocol based on a protocol established by Sun *et al. (40)*. Later, the procedures were modified to that described in section 2.8 to increase the yield of soluble stable variant proteins. The results of both methods are compared in this thesis.

Plasmid containing native or mutant *tyrA* gene (50-100 ng) was co-transformed with pMagik DNA into *E. coli* BL21(DE3) cells (see section 2.5). The resulting culture was plated on LB/agar containing ampicillin (100 μg/mL) and kanamycin (50 μg/mL) and then incubated overnight at 37°C. A single colony was selected and grown in 50 mL of LB medium supplemented with the same antibiotics overnight at 37°C with shaking and diluted into 1.5 L of the same medium. Cells continued to grow at 37°C until an OD_{600} of approximate 0.6, PD protein expression was induced by the addition of 0.4 mM of isopropyl-β-D-thiogalactopyranoside (IPTG). The culture was incubated further for 3 h at 23°C and then overnight at 18°C with shaking. Cells were harvested by centrifugation at 10000 x g at 4°C for 30 min and the cell pellet was frozen in -86°C freezer for 30 min before immediate processing or storage at -20°C. The freeze-thaw cycles facilitate the protein extraction. Purification of Δ19PD proteins was carried out on the bench but with ice-cold buffers. The cell pellet was resuspended in buffer A (50 mM Tris, 500 mM NaCl, 5% glycerol, pH 7.5) (4-6 mL/g of wet cell pellet) supplemented with 5 mM imidazole, Complete™ protease inhibitor cocktail tablet (one tablet per 50 mL of resuspension), 0.5 mM phenyl-methyl-sulfonyl fluoride (PMSF) and 1 mM benzamidine. Cells were firstly disrupted by homogenization with a Dounce glass pestle and then by passage through a Thermo Spectronic French Press at 18000 psi once. After the addition of more PMSF and

benzamidine, the sample was sonicated with a Branson 250 Sonifier for five bursts of 30 s with 1 min of cooling on ice between each burst. Insoluble cellular debris was removed by centrifugation at 100000 x g for 45 min at 4°C. The cell-free extract was applied to a column of 5 mL of Superflow Ni-NTA resin (binding capacity: 5-10 mg of His-tagged protein per mL resin) previously equilibrated with ice-cold buffer A containing 5 mM imidazole. The flow-through was collected and then the column was washed with 300 mL of buffer A containing 30 mM imidazole. Bound His-tagged protein was eluted with buffer A containing 300 mM imidazole and collected in one mL fractions supplemented with 1 mM EDTA. All column flow rates were 1 mL/min. Protein elution was monitored quantitatively by adding a sample aliquot to a drop of Bio-Rad dye. Those protein-containing fractions from the high imidazole wash were pooled and thrombin was added in a ratio of protease to pooled protein of 1:1000 (w/w). The sample was dialysed overnight at 4°C against buffer A containing 2.5 mM $CaCl_2$ in order to facilitate cleavage of the histidine tag. Any His-tagged protein that remained (due to incomplete digestion at the protease site) was removed by re-applying the thrombin-treated protein to the Ni-NTA column. If digestion was complete then the re-application was omitted. Purified Δ19PD proteins were concentrated if necessary using an Amicon centrifugal filter unit (MW cut-off 10 kDa) and stored in buffer A at -20°C. Each step of the purification was monitored by SDS-PAGE. Protein concentration was determined by the Bio-Rad Protein assay kit using BSA (Sigma) as a standard (see section 2.9).

2.8 Modification of the Expression and Purification of Δ19PD Proteins

Recombinant Δ19PD proteins were expressed and purified as described above but with some major modifications that together, increased the yield of soluble, stable variant Δ19PD proteins. First, DNA from pΔ19PD and pMagik were co-transformed in *E. coli* BL21(DE3)pLysS cells and growth was selected on LB/agar containing ampicillin (100 μg/mL), kanamycin (50 μg/mL) and chloramphenicol (20 μg/mL). Second, a single colony was incubated in 50 mL of antibiotic-containing medium at 37°C with shaking for 5 h. The culture was then diluted into 0.5 L of Overnight Express™ Instant TB Medium with ampicillin (100 μg/mL), kanamycin (50 μg/mL) and chloramphenicol (5 μg/mL) and further grown at 37°C with shaking overnight. Third, after centrifugation of the culture, the cell pellet was resuspended in BugBuster™ Extraction Reagent (5 mL/g of wet cell pellet) supplemented with Benzonase Nuclease (1 μL per 1 mL of BugBuster reagent) and Complete™ protease inhibitor cocktail tablet (one tablet per 50 mL of resuspension). Cells were disrupted by homogenization of the resuspension followed by intermittent gentle vortexing at room temperature for 20 min. Insoluble cellular debris was removed by centrifugation at 16000 x g for 45 min at 4°C. After application of the cell-free extract to the Ni-NTA column, the flow-through was re-circulated slowly through the resin assisted by a pump overnight. The flow-through was collected and the column was washed with buffer A containing 10 mM imidazole (200 mL) followed by 30 mM imidazole (1 L) before eluting PD with 300 mM imidazole. Additionally, all chromatography separations steps were performed in the cold room or at 4°C. Protein-containing fractions were pooled, digested with thrombin, dialysed, concentrated and stored as previously described in section 2.7.

2.9 Determination of Protein Concentration

Protein concentration was calculated using the Bio-Rad protein assay kit (Bio-Rad Laboratory) with bovine serum albumin (BSA, Sigma) as a standard. BSA was dissolved in 10 mM Tris-HCl, pH 7.4, filtered through a 0.2 μm syringe and its concentration was determined by Abs_{280} using an extinction coefficient of 0.667 mL/mg/cm (*58*).

2.10 Polyacrylamide Gel Electrophoresis

Sodium dodecyl sulfate polyacrylamide gel electrophoresis (SDS-PAGE) was used to separate proteins under denaturing conditions in order to assess protein purity and molecular weight. All reagents were purchased from BioShop at BioUltraPure or electrophoresis grade unless stated otherwise. SDS-PAGE was performed using a 5% stacking gel (pH 6.8) and 12% resolving gel (pH 8.8) as described by Sambrook and Russell (*56*). A 30% acrylamide stock solution was prepared by mixing 29% (w/v) acrylamide and 1% (w/v) N,N'-methylene-bis-acrylamide in warm distilled H_2O. Tris buffers (1.5 M at pH 8.8 and 1 M at pH 6.8) were prepared in distilled H_2O and adjusted to the appropriated pH with HCl. The acrylamide and Tris buffer solutions were stored at 4°C. Ten percent SDS (w/v) in distilled H_2O was stored at room temperature while 10% (w/v) ammonium persulfate was prepared weekly in distilled H_2O and was stored at 4°C. Electrophoresis buffer was prepared with 25 mM Tris base, 250 mM glycine and 0.1% SDS, pH 8.3. Protein samples, diluted with 2 x SDS gel-loading buffer (100 mM Tris-Cl pH 6.8, 4% SDS, 0.2% bromophenol blue and 20% glycerol), and unstained protein molecular weight marker (Fermentas) were boiled for 5 min before loading on the gel. Electrophoresis was started at 80V and then increased to 150V when the dye reached the

resolving gel. Proteins were visualized by staining with Brilliant Blue R Concentrate (0.25% (w/v) Brilliant Blue R, 40% (v/v) methanol and 7% (v/v) acetic acid, Sigma) followed by destaining in a solution of 50% (v/v) methanol, 7% (v/v) acetic acid and 3% (v/v) glycerol.

Native polyacrylamide gel electrophoresis was performed to determine the relative molecular weights of proteins under non-denaturing conditions. The procedures used are identical to those described for denaturing PAGE except for the following: a single resolving gel (7.5% acrylamide, pH 8.8) was used; electrophoresis buffer and loading dyes did not contain SDS. The migration of PD proteins was compared to those of native molecular weight standards (Invitrogen). MW markers were kindly donated by Dr. Bill Zerges.

2.11 Mass Spectrometry

The molecular weight of native and variant Δ19PD proteins was confirmed by ESI-ToF-MS. Samples were prepared for analysis using a protocol adapted by Manioudakis for the analysis of membrane-associated proteins (*59*). Details are as following: 100 μg of protein in 100 μL was mixed with 300 μL methanol, 100 μL chloroform, and 200 μL MilliQ water with 15 s of vortexing after the addition of each solvent. The sample was centrifuged at maximum speed for 3 min; the protein was present as a precipitate at the interface of the two phases. Both phases were carefully removed without disrupting the protein layer. The protein precipitate was then washed twice with 300 μL of methanol, vortexing for 15 s and centrifuging for 2 min between washes. After decanting the methanol, the protein pellet was air-dried at room temperature and protected from light.

The dried pellet was then resuspended in a solution of 30% methanol/0.2% formic acid (v/v) prior to injection and centrifuged for 5 min to remove any insoluble material. The samples were applied to a Micromass Q-ToF 2 triple-quadrupole mass spectrometer by direct injection at a flow rate of 1 μL/min. Samples were analyzed in the positive-ion mode within an *m/z*-range of 600-2600 using MassLynx 4.0 software (Waters Micromass). Instrument parameters were as following: source block temperature: 80°C; capillary voltage: 3.5 kV; cone voltage: 35 V; ToF: 9.1 kV; MC: 1.8 kV; resolution: 8000. Calibration of the instrument was performed with Myoglobin (Sigma).

2.12 Determination of Enzyme Activities and Kinetic Parameters

The oxidative decarboxylation of prephenate in the presence of NAD^+ was monitored at 340 nm as described by Turnbull *et al.* (*35*) using a Varian Cary 50 spectrophotometer equipped with a thermostated cuvette holder. The standard activity assays for Δ19PD proteins were conducted at 55°C in a total volume of 1 mL using a quartz cuvette with 1 cm path length as described by Bonvin *et al.* (*50*). Briefly, the reaction buffer containing 50 mM HEPES and 150 mM NaCl (pH 7.5) was incubated for 2 min at 55°C followed by the consecutive additions of NAD^+ and prephenate. The reaction was then initiated by addition of an appropriate amount of enzyme. The OD_{340} was recorded continuously for at least 1 min and reaction rates were calculated from the linear portion of progress curves using the software supplied with the spectrophotometer. Exact concentrations of substrates are listed in figure legends of the Results. Values of k_{cat} and K_m were obtained by fitting initial velocity data from substrate saturation curves to the Michaelis-Menten equation: $v_0 = (V_{max}[S])/([S] + K_m)$ using nonlinear least-squares

analysis provided by Grafit Software version 5.0 (Erathicus Software). The turnover number k_{cat} was calculated using the relationship: $k_{cat} = V_{max}/[\text{active site}]_{total}$ where V_{max} represents the specific activity recorded at saturating concentrations of substrates. A unit of enzyme is defined as the amount of enzyme required to give 1 μmol of product per min at the specified temperature. Units of activity, specific activity and k_{cat} were calculated as shown below:

$$\text{Units (}\mu\text{mol/min/mL)} = \frac{\Delta OD_{340}/\text{min}}{1\text{ cm} \times 6400\ M^{-1}\ cm^{-1}} \times \frac{10^6\ \mu\text{mol}}{\text{mol}} \times \frac{1\text{L}}{10^3\ \text{mL}} \times \text{dilution factor}$$

$$\text{Specific activity (}\mu\text{mol/min/mg)} = \frac{\text{Units}}{\text{mg/mL protein}}$$

$$k_{cat}\ (s^{-1}) = V_{max}\ (\mu\text{mol/s/mg}) \times \frac{33196\text{ mg}}{\text{mmol active site}} \times \frac{\text{mmol}}{10^3\ \mu\text{mol}}$$

2.13 Far-UV Circular Dichroism Spectroscopy

Far-UV CD spectra of wild-type and variant proteins were recorded on a Jasco-815 spectrometer in a 0.1cm path-length rectangular cell connected to a Peltier temperature control. Proteins were buffer exchanged into a PPS buffer (50 mM potassium phosphate, 75 mM NaCl, pH 7.5) and diluted to a concentration of 10.5 μM monomer. Spectra were recorded at 25°C by averaging 5 accumulations of scans from 260 nm to 200 nm using a scan rate of 100 nm/min, 0.25 s response time, a 0.2 nm step resolution, a bandwidth of 1

nm, and a sensitivity of 100 mdeg. The spectra were corrected for background signal from the buffer.

2.14 Fluorescence Spectroscopy

Fluorescence emission spectra of native and variant proteins were recorded at 25°C on an Aminco Bowman Series 2 Luminescence Spectrometer equipped with a temperature controlled cell holder or Shimadzu RF-5301PC Spectrofluorophotometer. Proteins were buffer exchanged into a PPS buffer and diluted to a concentration of 3 μM monomer. The excitation wavelength was set at either 280 nm or 295 nm, and the fluorescence emission was measured from 300 nm to 400 nm using a medium scan rate at excitation and emission bandwidths of 3 or 4 nm as indicated in the figure legends. A 1 cm (0.5 mL) fluorescence cuvette was used. The emission spectra were corrected for background signal from the buffer.

2.15 Effect of Denaturant on Enzyme Structure and Activity

The equilibrium denaturation of native and H217A proteins induced by guanidine-HCl (Gdn-HCl) was followed by measuring the changes in the far-UV CD signal at 222 nm or through tryptophan fluorescence emission. An 8 M Gdn-HCl stock solution was prepared in PPS buffer, adjusted to pH 7.5 and passed through a 0.45 μm filter. Samples (1 mL) at each Gdn-HCl concentration (0-6 M in 0.5 M increments) were obtained by mixing PPS buffer and the 8 M Gdn-HCl stock solution in the appropriate ratio and adding the enzyme also in PPS buffer to a final concentration of 3 μM. The samples

were equilibrated at room temperature for 20 h in capped Eppendorf tubes as outlined by Bonvin *et al.* (*50*). Ellipticities at 222 nm were measured in a 0.1 cm path-length cell using the parameters listed in section 2.13. Fluorescence emission scans were recorded at an excitation λ of 295 nm and using the parameters listed in section 2.14. All CD and fluorescence data were corrected for contribution by the buffer. CD or fluorescence measurements were converted to percent folded using the following relationship:

$$f_F = (y_F - y_X)/(y_F - y_U)$$

Where f_F refers to fraction folded, y_F or y_U represent the values of the spectroscopic signals at 0 M (folded) and 6 M Gdn-HCl (unfolded) and y_X represents the values at the different concentrations of Gdn-HCl.

To examine the effects of low concentrations of Gdn-HCl on Δ19PD activity, native enzyme (10 μg) and H217A (240 μg), previously exchanged into PPS buffer, were incubated in the reaction buffer for 2 min at 30°C containing 0 M, 0.5 M and 1 M Gdn-HCl. NAD^+ (2 mM) was added, and then the reaction was initiated by the addition of prephenate (1 mM for native enzyme and 4 mM for H217A). Reaction rates were calculated as described in section 2.12.

2.16 Determination of Thermal Stability

Native enzyme (100 μL of sample at 0.9 mg/mL) and H217A enzyme (400 μL at 1 mg/mL) in 50 mM HEPES/150 mM NaCl were placed in capped Eppendorf tubes. Protein thermal stability was monitored by incubating tubes in a water bath set at 95°C. At specific time intervals, tubes were removed, cooled on ice for 2 min, centrifuged at

maximum speed for 5 min at room temperature, and then the supernatants were decanted into fresh Eppendorf tubes. Protein concentrations of the samples were determined by using the Bio-Rad reagent and PD activities were determined at 55°C by the standard assay as outlined in section 2.12 using 5 μL of native enzyme or 80 μL of H217A. The concentration of NAD^+ in the assay was fixed at 2 mM while prephenate was either 1 mM (for wild-type) or 4 mM (for H217A).

The thermal denaturation of native enzyme and H217A variant was followed by monitoring the loss of secondary structure by far-UV CD. CD measurements were recorded at 222 nm from 25°C to 95°C using a temperature ramping program controlled by Jasco 815 spectrometer. Parameters were set at ΔT of 40°C/h, a 0.2°C step resolution, and a 0.25 s response time. Proteins in buffer A were directly diluted into 50 mM potassium phosphate, 500 mM NaCl, pH 7.5, to a final concentration of 16.6 μM monomer.

2.17 Determination of the effect of L-tyrosine and *m*-fluoro-DL-tyrosine on Δ19PD Activity

The effect of L-tyrosine on the activity of native and variants of Δ19PD were measured in a reaction volume of 1 mL. A stock solution of 10 mM L-tyrosine in reaction buffer was prepared fresh with the addition of heat for a few minutes and the pH was re-adjusted to pH 7.5 with NaOH. Assays were carried out in the presence of 0-9 mM of L-tyrosine by mixing the reaction buffer and the tyrosine stock solution in the appropriate ratio to reach the desired concentrations of L-tyrosine. The resulting solution was

incubated at 55°C for 2 min followed by the consecutive addition of NAD^+ and prephenate, and then the reaction was initiated by addition of an appropriate amount of enzyme. Substrate concentrations used were 2 mM NAD^+ and approximately 4 x K_m for prephenate unless otherwise stated. Reaction rates were calculated as described in section 2.12.

Assays in the presence of *m*-fluoro-DL-tyrosine were performed as described above but using a stock solution of *m*-fluoro-DL-tyrosine that had been dissolved in 0.5 M HCl. Various concentrations of *m*-fluoro-DL-tyrosine were prepared by diluting the stock solution with a buffer containing 50 mM HEPES, 50 mM Tris and 150 mM NaCl, at an appropriate pH. Preliminary trials were conducted by adding acid to the above buffer in order to calculate the initial pH of the incubation buffer required to produce a final pH of 7.5. Activities were recorded as described for the assay with L-tyrosine except prephenate concentrations of approximately 4 x K_m for native enzyme and approximately K_m for H217A were used.

Chapter 3: Results

In this thesis, active site variants of a crystallizable form of the tyrosine biosynthetic enzyme prephenate dehydrogenase (Δ19PD) from *Aquifex aeolicus* were expressed and purified with special attention devoted to improvements of the purification scheme. Biochemical and biophysical studies were then employed to help assign roles for specific residues (His217, Lys246 and Arg250) in the catalytic mechanism and structure of the enzyme. Additionally, the fluorescence properties of *A. aeolicus* Δ19PD were also probed through the analysis of variants.

3.1 Site-Directed Mutagenesis

A portion of *tyrA* from *A. aeolicus* had been previously cloned into the *E. coli* expression vector pET15b between the *Nde*I and *Bam*HI restriction sites to construct the pΔ19PD plasmid encoding a removable N-terminal hexahistidine tag (*40*). Thus, the recombinant plasmid is approximately 6.6 kbp including a 5708 bp pET15b vector and an 886 bp insert. To obtain protein variants W190F, K246Q/A, R250Q/A/K, and W259F, site-directed mutagenesis was performed on *tyrA* using the QuikChange™ method of Stratagene. Mutants were selected by digestion with *Dpn*I which cleaves fully methylated or hemi-methylated template DNA but not DNA synthesized during the mutagenesis reaction. After transforming the PCR products into XL-10 Gold *E. coli* cells that can repair the nicked mutagenic strand, plasmid preparations were performed on selected colonies. The presence of *tyrA* in the transformants was verified by restriction analysis (see 886 bp insert in Figure 8) and the mutant DNAs were sent to Bio S&T for

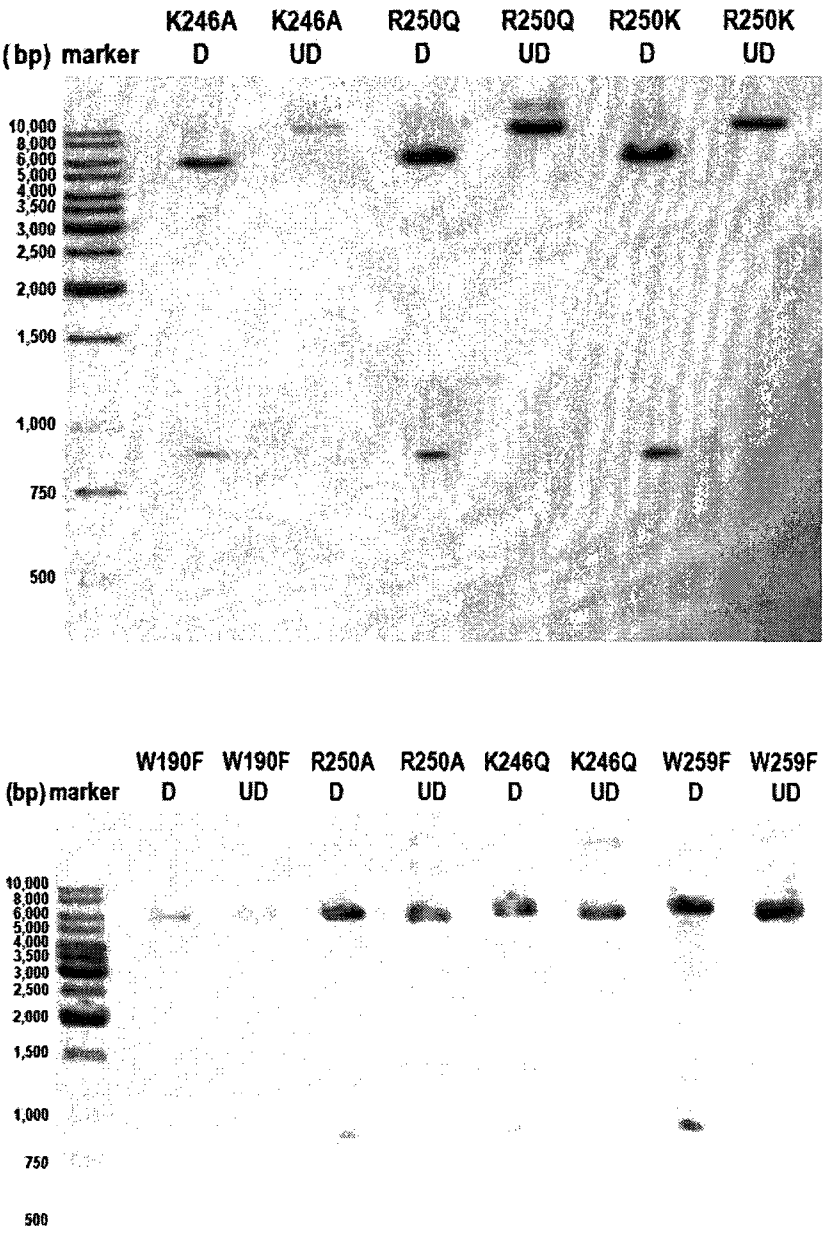

Figure 8: Electrophoretic analysis of mutant plasmid DNA of *A. aeolicus* Δ19PD generated by QuikChange™ site-directed mutagenesis.

D = digested plasmid; UD = undigested plasmid; bp = base pair.

sequencing of both strands of the insert. Sequencing results confirmed that all mutant plasmids carried the desired base change(s) and that no additional mutations had been introduced. The H217A mutation was previously constructed by J. Bonvin although the purification and characterization of the variant protein is described in this thesis. W259F Δ19PD mutant plasmid was constructed in this work but the variant is being characterized elsewhere.

3.2 Expression and Purification Strategies of Native and Variant Δ19PD Proteins

The following eight Δ19PD proteins (native, W190F, H217A, K246Q/A and R250Q/A/K) were expressed and purified. The purification procedure used initially was based on the protocol originally developed for native Δ19PD as outlined by Bonvin *et al.* (*50*) and Sun *et al.* (*40*). Briefly, plasmids pΔ19PD and pMagik were co-transformed into *E. coli* BL21(DE3) cells which were then grown in LB medium, and recombinant protein expression was induced by IPTG. Cells were disrupted by high pressure and sonication in the presence of protease inhibitors and recombinant Δ19PD proteins were purified using Ni-NTA affinity chromatography. The affinity tag was then removed by cleavage with thrombin during a dialysis step. In the revised protocol, the plasmids were co-transformed into *E. coli* BL21(DE3)pLysS cells which allows for tighter control of protein expression. The cells were then cultured at 37°C in Overnight Express™ Instant TB Medium which promotes protein expression by an auto-induced system. Cells were disrupted with minimal shearing using BugBuster™ Extraction Reagent and then purified by Ni-affinity chromatography at 4°C.

Although the former protocol afforded adequate expression of native Δ19PD (*51*), preparations of some variants resulted in lower yields and/or variable levels of purity (discussed later). With the revised protocol, however, yields of Δ19PD proteins were consistently higher, in smaller culture volumes, and could be routinely purified to homogeneity without proteolysis. In both procedures heat treatment of the cell-free extract was omitted.

Protein purification was monitored by activity assays and SDS-PAGE. Figure 9A and 9B and Table 4A and 4B show a comparison of the purification of R250Q using the two protocols: the revised (A) and the original (B) protocols. The predicted size of the His-tagged R250Q Δ19PD monomer is ~ 35 kDa. Over-expression of the variant protein using the modified procedure is evident in the cell lysate and cell-free extract from just 0.5 L of culture (Figure 9A, lanes 1 and 2). The cell-free extract was re-circulated through the Ni-NTA affinity column at 4°C for several hours to ensure efficient binding of the His-tagged protein. Accordingly, no proteins were observed in the column flow-through (lane 3) or in the extensive wash steps with buffer containing 10 mM or 30 mM imidazole (lanes 4 and 5). Pure His-tagged variant eluted from the column in a wash containing 300 mM imidazole (lane 6). Incubation with thrombin yielded a protein whose mobility shift was consistent with the removal of the 14 residue tag (lane 7).

By comparison, R250Q Δ19PD appeared as a much smaller fraction of the total cellular protein or cell-free extract (Figure 9B, lanes 2 and 3) when processed from a 4.5 L culture using the original procedure. Additionally, the chromatography conditions resulted in poor retention of R250Q on the Ni-affinity column (note the 33 kDa band in the flow-through (lane 4) and 30 mM imidazole wash (lane 5)). Although SDS-PAGE

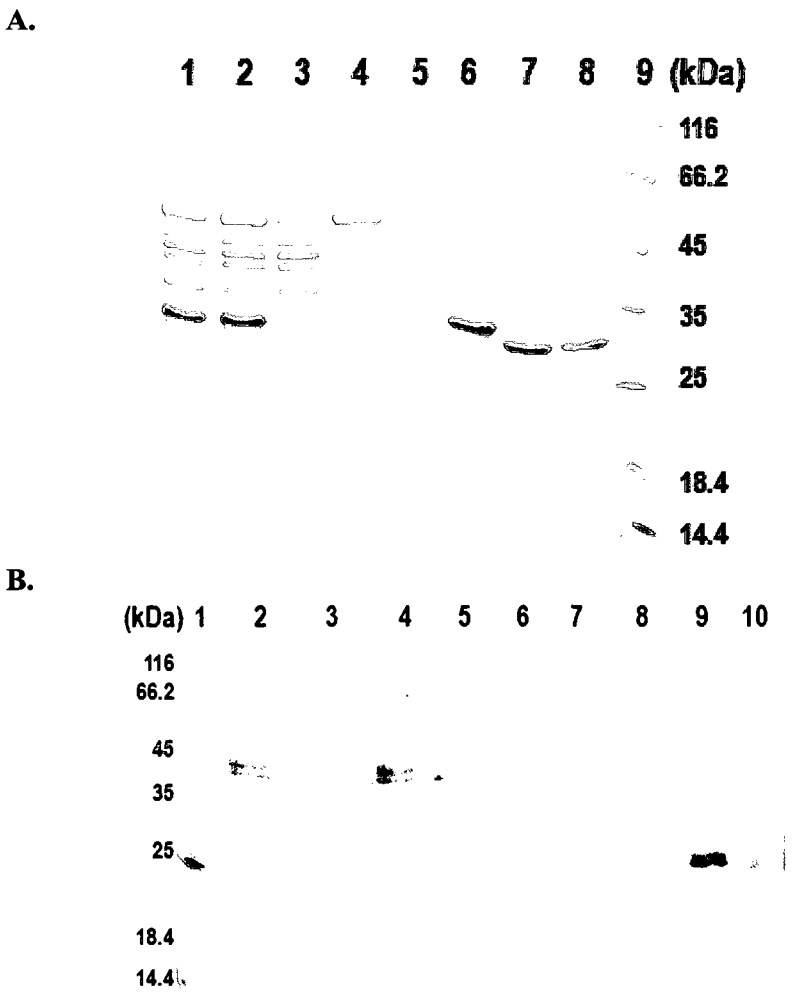

Figure 9: SDS-PAGE analysis of the purification of R250Q Δ19PD

(A). Purification using the revised protocol. Lane 1: Cell lysate (27 μg), Lane 2: Cell-free extract (28 μg), Lane 3: Ni-NTA flow-through (24 μg), Lane 4: 10 mM imidazole first wash (12 μg), Lane 5: 30 mM imidazole last wash (0 μg), Lane 6: Pool from 300 mM imidazole wash (5 μg), Lane 7: Thrombin-treated (4 μg), Lane 8: wild-type Δ19PD (3 μg), Lane 9: Molecular weight ladder.

(B). Purification using the original protocol. Lane 1: Molecular weight ladder, Lane 2: Cell lysate (15 μg), Lane 3: Cell-free extract (15 μg), Lane 4: Ni-NTA flow-through (15 μg), Lane 5: 30mM imidazole first wash (15 μg), Lane 6: 30mM imidazole second wash (2 μg), Lane 7: 30mM imidazole third wash (0.3 μg), Lane 8: 30mM imidazole last wash (0 μg), Lane 9: Pool from 300 mM imidazole wash (6 μg), Lane 10: Thrombin-treated (5.5 μg).

Table 4: Purification table for R250Q Δ19PD

1A:

	Total protein (mg)	Total activity[a] (Units)	Specific activity[a] (Units/mg)	Activity yield (%)	Purification fold
Cell-free extract	228	209	0.915	100	1.00
Ni-NTA flowthrough	120	10.2	0.085	4.9	0.09
10 mM imidazole wash	30.8	1.7	0.054	0.8	0.06
Ni-NTA pooled	24.9	192	7.69	91.9	8.41
Thrombin-treated	10.4	130	12.5	62.1	13.7

1B:

	Total protein (mg)	Total activity[b] (Units)	Specific activity[b] (Units/mg)	Activity yield (%)	Purification fold
Cell-free extract	1780	205	0.115	100	1.00
Ni-NTA flowthrough	1646	116	0.070	56.5	0.61
30 mM imidazole wash	162	10.5	0.065	5.1	0.57
Ni-NTA pooled	6.0	7.4	1.24	3.6	10.8
Thrombin-treated	4.9	6.7	1.37	3.3	11.9

(1A): from a 0.5 L of Overnight Express™ Instant TB culture of *E. coli* BL21(DE3)pLysS harbouring pΔ19PD using the revised purification procedures. **(1B)**: from a 4.5 L of LB culture of *E. coli* BL21(DE3) harbouring pΔ19PD using original purification procedures. [a] Activity assays were performed at 55°C at 2 mM of NAD^+ (> 10 x K_m) and 1 mM of prephenate (~ K_m). [b] Activity assays were performed at 55°C at 2 mM of NAD^+ (> 10 x K_m) and 10 mM of prephenate (~ 4 x K_m). Units = μmol/min.

analysis indicated that the column was sufficiently washed to remove any protein contaminants (lane 8), PD that eluted in the 300 mM imidazole wash was impure (lane 9). In this preparation, treatment with thrombin appeared inefficient (lane 10). Table 4 also mirrors the findings obtained by SDS-PAGE analysis of the purification of R250Q. The table shows that a high proportion of active protein was not retained by the affinity column and that the specific activity of the final preparation was considerably lower than when using the revised protocol.

A summary of the yields of all Δ19PD proteins characterized in this thesis are given in Table 5. Of the four proteins purified using both protocols, the total protein in the cell-free extract and pooled protein after the high imidazole wash were considerably improved using the revised procedure. In particular, W190F's expression was remarkably improved as deduced by activity and protein assays and SDS-PAGE analysis (data not shown). All purified proteins after Ni-affinity chromatography and thrombin treatment were analyzed by SDS-PAGE as shown in Figure 10.

Table 5: Purification summary for native and variant Δ19PDs

Protein	Total protein in cell-free extract (mg/L of culture)	Pooled protein [a] (mg/L of culture)	Specific activity[b] (U/mg)
Native	40 [c]	10	8.56
	1528 [d]	192	7.00
H217A	71 [c]	26	0.38
	1239 [d]	112	0.45
W190F	110 [c]	1.5	11.1
	1257 [d]	57	12.7
R250Q	482 [c]	1.3	1.37
	456 [d]	50	12.5
R250A	1672 [d]	70	14.0
R250K	737 [d]	46	13.5
K246Q	589 [d]	25	9.67
K246A	1080 [d]	92	11.8

[a] Final elution from Ni-NTA affinity column. [b] Activity assays of thrombin-treated sample were performed at 55°C at a saturating concentration of NAD^+ (2mM) and various concentrations of prephenate (1 mM for native enzyme, W190F, R250Q, R250A, R250K and K246Q, 2 mM for K246A and 4 mM for H217A). [c] Original protocol for expression and purification . [d] Revised protocol for expression and purification.

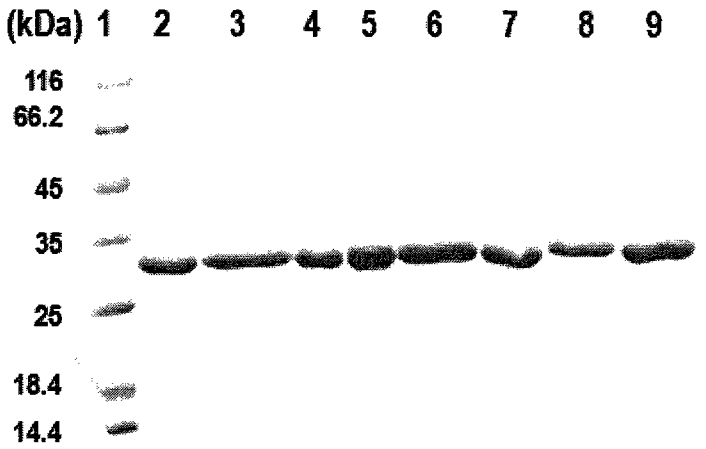

Figure 10: SDS-PAGE analysis of purified Δ19PD proteins using the revised protocol

Lane 1: Molecular weight ladder, Lane 2: native enzyme, Lane 3: H217A, Lane 4: W190F, Lane 5: R250Q, Lane 6: R250A, Lane 7: R250K, Lane 8: K246Q, and Lane 9:K246A. Between 5 and 6 μg of protein were loaded in lanes 2-9. Protein samples after Ni-NTA affinity chromatography and treatment with thrombin were analyzed on a 12% polyacrylamide gel as outlined in section 2.9.

3.3 Electrospray Ionization Mass Spectrometry

The purified Δ19PD proteins were analyzed by ESI-Q-ToF MS in order to confirm that the amino acid substitutions generated by the site-directed mutagenesis were correct. Table 6 summarizes the theoretical mass values of each thrombin-treated protein calculated using the program EXPASY and the experimental mass values generated using MassLynx. These results were in excellent agreement; thus, the desired amino acid substitution in each variant protein was correct. A representative mass spectrum of R250Q was shown in Figure 11A. The excellent quality of the spectrum mirrors the high sample purity. In contrast, a much poorer quality mass spectrum was obtained for the thrombin-treated R250Q variant purified using the original protocol (Figure 11B). Interestingly, the only major peak observed from this sample was at $[M+H]^+$ of 32886 Da which corresponds to a protein produced by cleavage immediately preceding Δ19PD's start methionine rather than between arginine and glycine of the thrombin recognition site. It is likely that R250Q Δ19PD is susceptible to proteolysis under the original expression and purification conditions.

Table 6: Molecular weight summary of purified thrombin-treated wild-type and variant Δ19PDs using revised protocol

Δ19PDs	Expected Mass [a] (Da)	Observed Mass (Da)	Difference (Da)
Wild-type	33196.50	33196.20	0.30
H217A	33130.44	33129.60	0.84
W190F	33157.47	33157.20	0.27
R250Q	33168.45	33167.90	0.55
R250A	33111.39	33110.50	0.89
R250K	33168.49	33167.60	0.89
K246Q	33196.46	33195.30	1.16
K246A	33139.41	33139.00	0.41

[a] Expected mass calculated using EXPASY-PeptideMass program which gives the average molecular weight of the deprotonated side chain

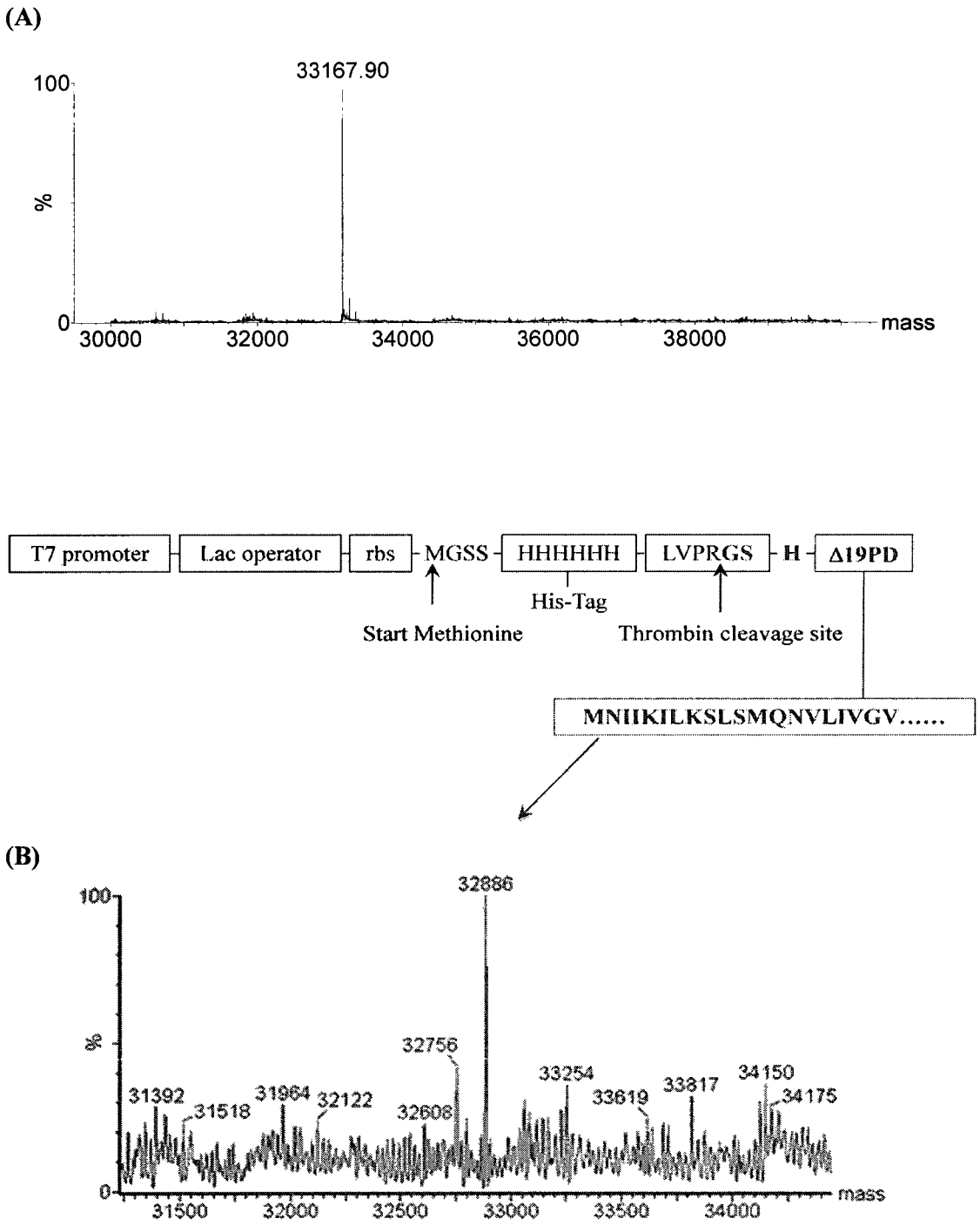

Figure 11: Deconvoluted ESI-MS spectra of R250Q protein.

R250Q purified using the revised (A) and original (B) protocols. See section 2.10 for experimental details. The peak shows the molecular weight of the protein monomer.

3.4 Determination of the Global Secondary and Tertiary Structure of Native and Variant Δ19PD Proteins

3.4.1 Far-UV Circular Dichroism Spectroscopy

To determine if the amino acid substitutions at Trp190, His217, Lys246 and Arg250 affected the secondary structure of Δ19PD, far UV-circular dichroism (CD) spectroscopy was used. In the far-UV CD, polarized light is absorbed by amide and carbonyl groups in the protein peptide backbone; the degree of absorption of the different components of circularly polarized light depends on the configuration of the protein backbone (*60*). CD spectra were recorded at room temperature from 260-200 nm (Figure 12) revealing absorption minima at 209 and 222 nm which is characteristic of proteins with considerable α-helical content. Moreover, the spectra of all the proteins were virtually superimposable indicating that the global secondary structure of the proteins was not affected by the amino acid changes.

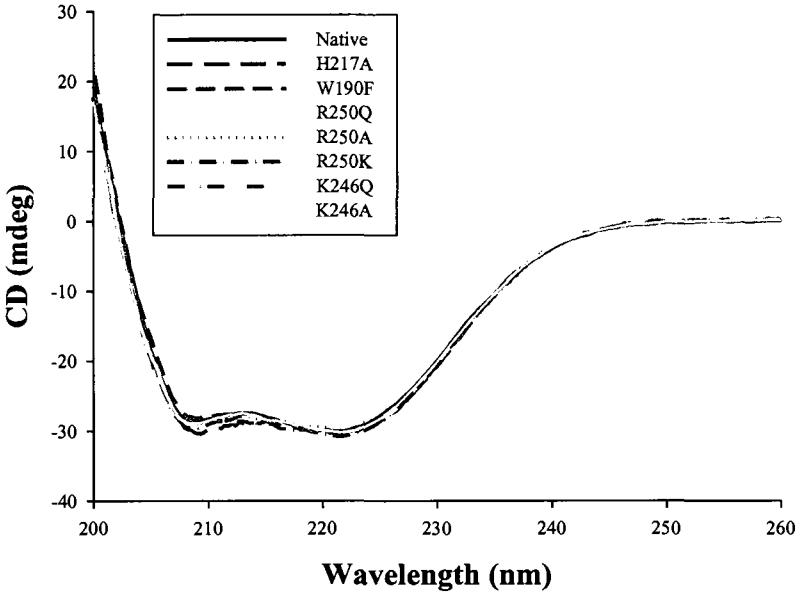

Figure 12: Far-UV CD spectra of native and variant Δ19PDs

Proteins (10.5 μM monomer) were in 50 mM potassium phosphate, 75 mM NaCl, pH 7.5. Spectra were recorded at 25°C in a 0.1 cm path-length rectangular cell with a scan rate of 100 nm/min. Each curve presents the average of 5 accumulations.

3.4.2 Fluorescence Spectroscopy

Fluorescence emission spectroscopy reveals information about the tertiary structure of a protein by probing the environments of the aromatic chromophores (tryptophan and tyrosine) and in particular the polarity of the regions surrounding these residues (*60*). *A. aeolicus* Δ19PD has 2 tryptophan residues and 10 tyrosine residues per monomer (*50*). At an excitation wavelength (λ_{ex}) of 280 nm both tryptophan and tyrosine residues contribute to the fluorescence emission while at λ_{ex} of 295 nm the fluorescence emission originates almost exclusively from tryptophan residues. Therefore, the fluorescence intensity is higher at a λ_{ex} of 280 nm than at a λ_{ex} of 295 nm. In addition, resonance energy transfer from tyrosine to tryptophan groups usually ensures that tryptophan fluorescence emission predominants.

The fluorescence emission spectra of Δ19PD proteins are represented in Figure 13A. Native and H217A proteins are shown in A, while the native protein and all other variants are shown in B. For most proteins the spectra show unusual double maxima at 317 nm and 330 nm. This has been interpreted as due to slightly different environments for the two tryptophan/monomer of Δ19PD (*50*). Moreover, the spectra of the variants (except W190F) are virtually superimposable indicating that these amino acid replacements have not perturbed the environment of tryptophan residues in the protein. Even though the crystal structure of *A. aeolicus* Δ19PD shows that Trp259 is adjacent to His217 (*40*), the conversion of His217 to alanine did not perturb the environment of Trp259 (Panel A). As expected, when Trp190 was changed to a phenylalanine, a residue that is non-polar and has a low quantum yield, the fluorescence intensities recorded from excitation at 280 or 295 nm are significantly reduced for the variant (see Panel B).

Interestingly, compared to the native protein or the other variants, the wavelength of maximal intensity for W190F has shifted to a single peak at ~ 330 nm.

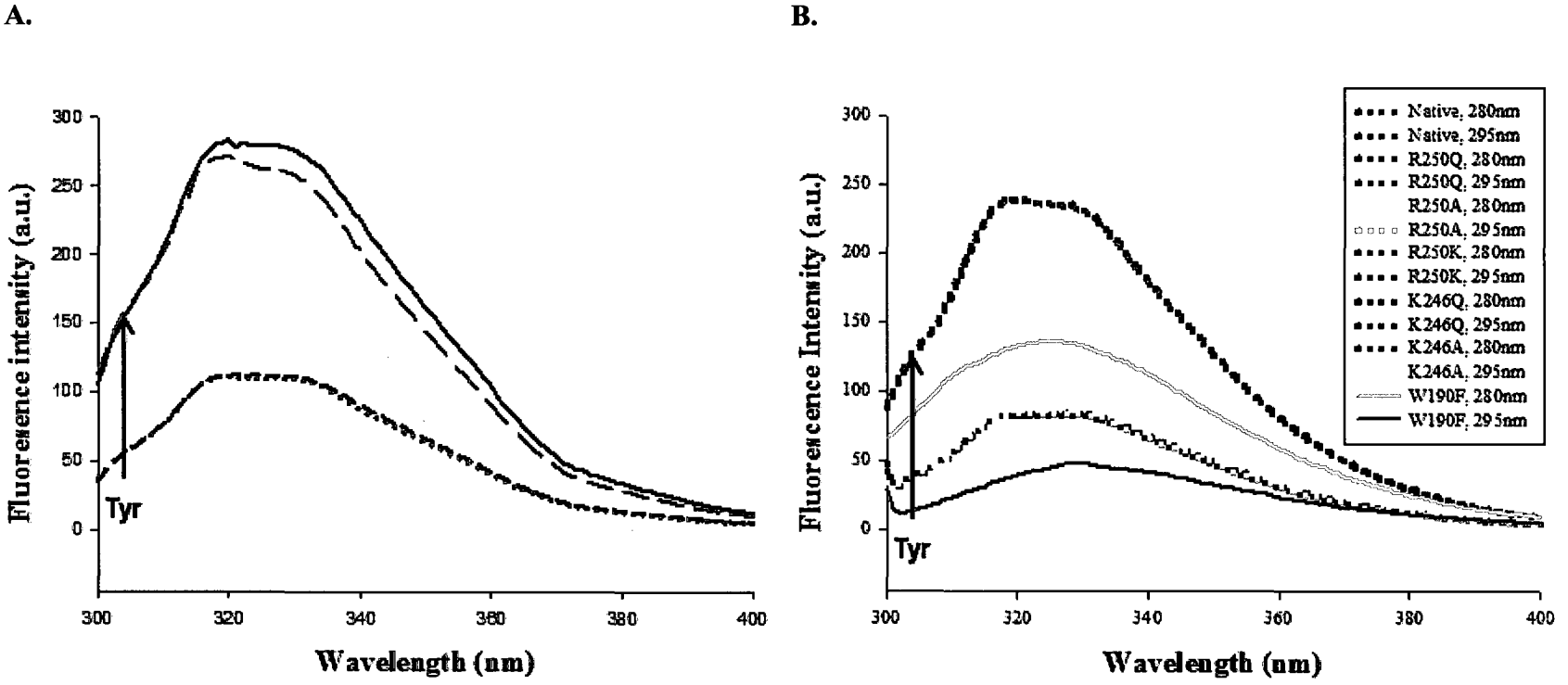

Figure 1: Fluorescence emission spectra of native and variant Δ19PDs

(A). Proteins (3 μM monomer) were in a buffer containing 50 mM potassium phosphate, 75 mM NaCl, pH 7.5. The excitation wavelength was set at 280 nm or 295 nm. Spectra were recorded at 25°C using excitation and emission bandwidths of 4 nm. Solid line (blue): H217A, excited at 280 nm; Short dashed line (black): H217A, excited at 295 nm; Long dashed line (pink): native, excited at 280 nm; Dotted line (red): native, excited at 295 nm.

(B). Proteins (3 μM monomer) were in a buffer containing 50 mM potassium phosphate, 75 mM NaCl, pH 7.5. Excitation wavelength was set at 280 nm or 295 nm. Spectra were recorded at 25°C using excitation and emission bandwidths of 3 nm. In both panels A and B, the peak (303 nm) corresponding to the contribution of tyrosine to the overall protein fluorescence emission is shown by the arrow.

3.5 Kinetic Studies of Native Δ19PD and Variants

3.5.1 Determination of Steady-state Kinetic Parameters

In order to determine the importance of selected active site residues of Δ19PD in the mechanism of the reaction, steady-state kinetic assays were performed on the variant proteins. Arg250, His217 and Lys246' are cationic residues reported in some but not all crystallographic data sets to be close to, or interact directly with the substrate and/or the product of the reaction, HPP (*40, 41*). Thus, these residues were substituted for side chains that were either non-polar (Ala), were polar but not charged (Gln), or were cationic but with a slightly shorter chain length (Lys). Trp190, which is near the NAD^+ binding site, was changed to a smaller non-polar residue (Phe). Substrate saturation curves were constructed from initial rates with prephenate or NAD^+ as the variable substrate. Representative graphs of both saturation curves are shown in Figure 14 for R250Q. Analysis of the data yield the kinetic parameters summarized in Table 7. The Michaelis constant (K_m) loosely reflects the affinity that the enzyme has for a substrate while the turnover number k_{cat} describes the rate at which the enzyme can convert substrate to product when the active site is saturated with substrate. The ratio of k_{cat}/K_m reflects the overall efficiency of the enzyme as a catalyst.

Arg250 was replaced by a glutamine, alanine, or lysine to probe the interaction with the negatively charged carboxylate groups of prephenate. The glutamine substitution caused a 13-fold increase in K_m for prephenate as did, surprisingly, the alanine replacement. In contrast, the K_m for prephenate decreased by 3-4 fold for the lysine variant compared to R250Q/A, but did not fully restore prephenate binding to the level seen for the native enzyme. These amino acid substitutions did not markedly affect values

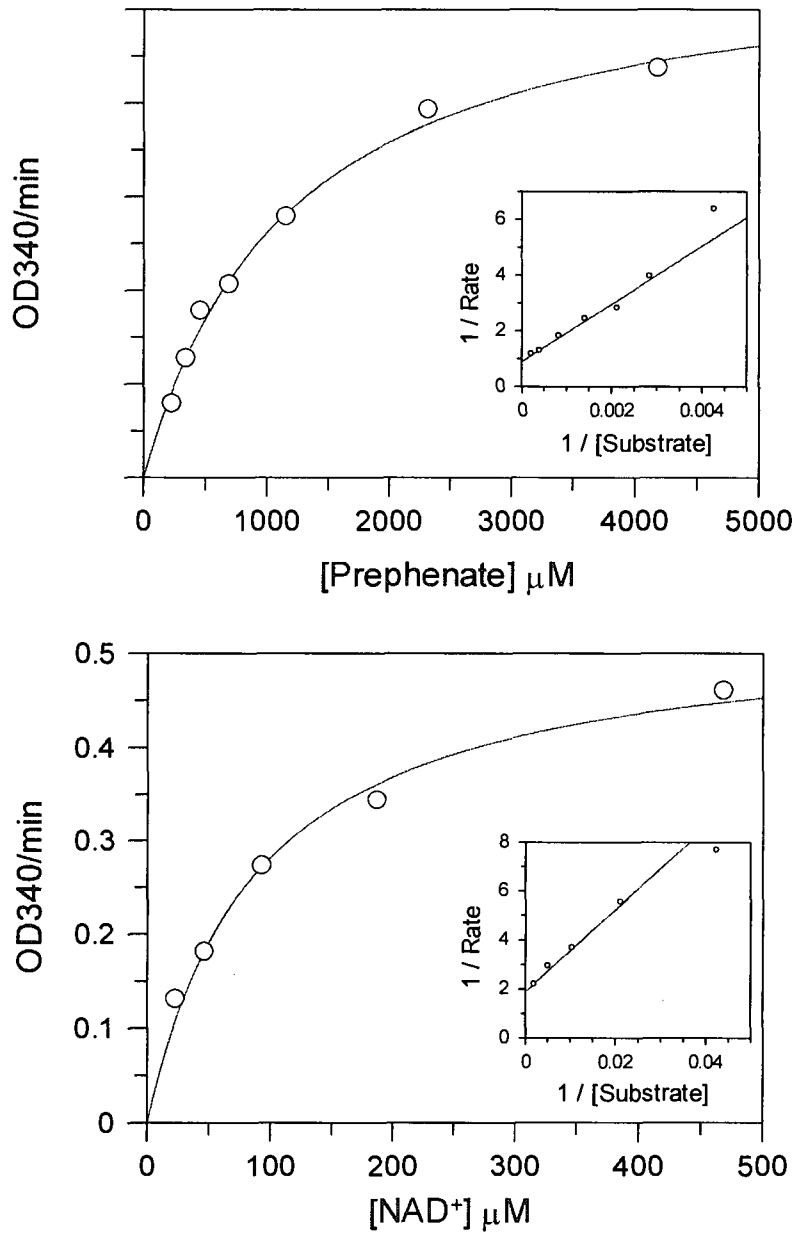

Figure 14: Representative substrate saturation curves for the reaction catalyzed by R250Q Δ19PD
Assays were carried out at 55°C in reaction buffer containing 50 mM HEPES and 150 mM NaCl, pH 7.5. When prephenate was the variable substrate, NAD^+ was fixed at 2 mM; when varying the concentration of NAD^+, prephenate was fixed at a concentration of 6 mM (~ 4 x K_m). Curves were generated by fitting initial velocity data to the Michaelis-Menten equation using Grafit Software. Double reciprocol plots (inset) were used to monitor any deviation from linearity.

Table 7: Kinetics parameters for reaction catalyzed by native and variant Δ19PD proteins

Variable Substrate[a]	Prephenate			NAD^+		
Protein	K_m (μM)	k_{cat} (s^{-1})	k_{cat}/K_m (M^{-1}/s)	K_m (μM)	k_{cat} (s^{-1})	k_{cat}/K_m (M^{-1}/s)
Native	85 ± 5.8	15.0 ± 0.3	1.8×10^5	58 ± 5.9	13.7 ± 0.47	2.34×10^5
H217A	3507 ± 194	0.4 ± 0.01	1.1×10^2	29 ± 1.1	0.4 ± 0.002	1.4×10^4
W190F	54± 4	8.0 ± 0.16	1.5×10^5	32 ± 2.8	8.8 ± 0.17	18×10^4
R250Q	1185 ± 118	9.9 ± 0.42	8.4×10^3	89 ± 12.6	11.6 ± 0.60	1.3×10^5
R250A	1130 ± 55	13.5 ± 0.22	1.2×10^4	71 ± 3.6	11.0 ± 0.13	1.5×10^5
R250K	301 ± 7	11 ± 0.07	3.7×10^4	33 ± 2.1	8.7 ± 0.13	2.6×10^5
K246Q	557 ± 40	14.4 ± 0.32	2.6×10^4	91 ± 6.2	11.1 ± 0.21	1.2×10^5
K246A	1854 ± 176	16.0 ± 0.54	8.6×10^3	120 ± 2.7	11.4 ± 0.07	9.5×10^4

[a] Reactions were performed at pH 7.5 and 55°C. Values were calculated from initial rates using a minimum of five NAD^+ concentrations ranging from 4-fold K_m up to 30-fold K_m for the variable substrate. When prephenate was the variable substrate NAD^+ was fixed at 2 mM, while when NAD^+ was the variable substrate, prephenate was fixed at 0.35 mM (native), 18 mM (H217A), 2 mM (W190F), 6 mM (R250Q), 4 mM (R250A), 1.25 mM (R250K), 2.2 mM (K246Q) and 7.36 mM (K246A).

for k_{cat} or K_m for NAD^+. Taken together, the data reveal that a protonated residue at position 250, but ideally the guanidinium group of arginine, was important solely in the binding of prephenate.

Lys246 is believed to interact with the ring carboxylate group of prephenate as suggested by the crystal structure at pH 3.2 of *A. aeolicus* Δ19PD complexed with NAD^+ and prephenate modeled in the active site (*40*) (Figure 7). Kinetic analysis at pH 7.5 showed that the conversion of lysine to glutamine at position 246 modestly increased the K_m for prephenate (6-fold) while the alanine substitution caused a ~ 20-fold increase in the K_m for prephenate. As with the substitution at Arg250, the K_m for NAD^+ and the k_{cat} were not markedly affected in the K246Q/A variants, and thus indicated that Lys246 plays a role only in prephenate binding.

Trp190, a residue which is believed to have no direct interactions with either NAD^+ or prephenate, was replaced by phenylalanine in order to determine its effect on protein fluorescence emission. As expected, the W190F variant showed kinetic parameters that were comparable to those of the native enzyme.

His217 is near the side chain carbonyl group of HPP and adjacent to Trp259 in the active site as shown in the crystal structure at pH 7.5 (*41*). The H217A variant showed remarkable changes in kinetic parameters. The alanine substitution caused a 30-fold increase in the K_m of prephenate and a ~ 40-fold decrease in k_{cat}. The binding of NAD^+ was not markedly affected. Overall, the catalytic efficiency of the variant is reduced by over three orders of magnitude reflecting His217's importance in prephenate binding and catalysis.

3.5.2 Inhibition of *A. aeolicus* Δ19PD Activity by L-tyrosine and *m*-fluoro-DL-tyrosine

To determine the effect of amino acid substitution on the regulation of PD activity by L-tyrosine, initial rates were recorded at 55°C in the presence of 0 to 9 mM L-tyrosine while keeping substrate concentrations constant. NAD^+ was fixed at 2 mM (> 10 x K_m) and prephenate was held at ~ 2 to 4 x its K_m value. A plot of percent residual activity as a function of the tyrosine concentration is shown in Figure 15. Although the variants were inhibited to different degrees by tyrosine, they can be grouped into three categories: those that were more inhibited by tyrosine (K246Q/A), those that were significantly less inhibited (R250Q/A/K and W190F), and H217A which appeared to be almost completely resistant to feedback inhibition by L-tyrosine. Approximate IC_{50} values (concentration of L-tyrosine required to reduce activity by 50%) are listed in the figure legend.

Since tyrosine's effective concentration in the assay was limited by its poor solubility, PD activity of H217A was also determined in the presence of the fluorinated analogue (*m*-fluoro-DL-tyrosine) which is reported to be a more potent inhibitor of TyrA proteins (*28, 45*). As shown in Figure 16, H217A ***is*** sensitive to feedback inhibition by *m*-fluoro-DL-tyrosine and as expected the native enzyme is significantly more inhibited. By 1 mM of the analogue, native enzyme is essentially inactive while H217A has retained 50% of its original activity.

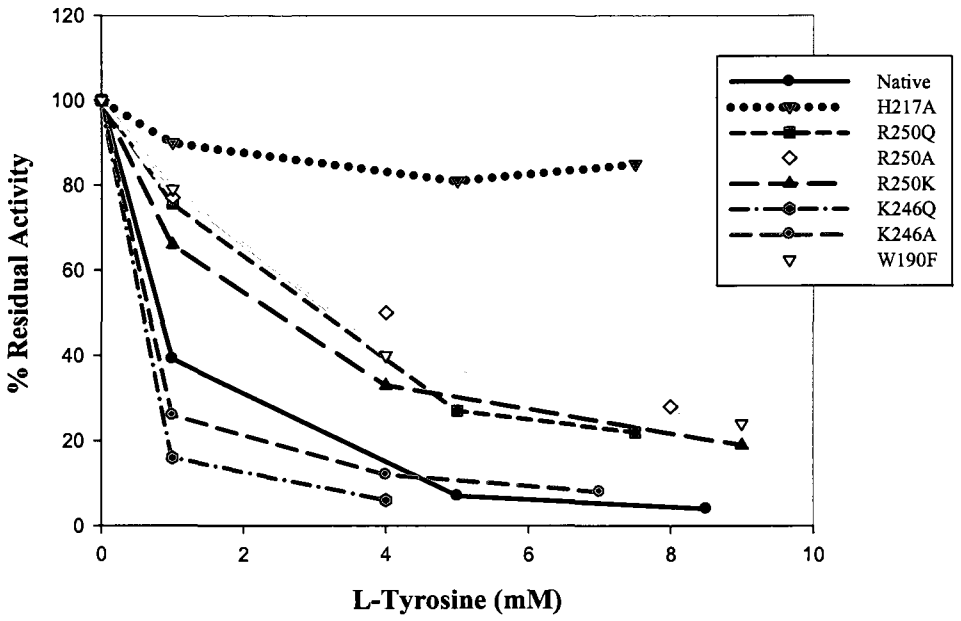

Figure 15: Effect of L-tyrosine on PD activity of native and variant forms of Δ19PD

Assays were carried out at 55°C in the presence of L-tyrosine (0-9 mM) in reaction buffer containing 50 mM HEPES, 150 mM NaCl, pH 7.5, and substrate concentration of 2 mM NAD^+ and ~ 4 x K_m for prephenate for native enzyme (0.6 mM), R250Q (5 mM), R250A (4.3 mM), R250K (1.4 mM), K246Q (2.2 mM), W190F (0.3 mM), ~ K_m for H217A (4 mM) and ~ 3 x K_m for K246A (6.3 mM). Approximate IC_{50} values for native enzyme, W190F, R250Q, R250A, R250K, K246Q and K246A are 0.9 mM, 3.2 mM, 3.1 mM, 4 mM, 2.5 mM, 0.6 mM and 0.7 mM, respectively.

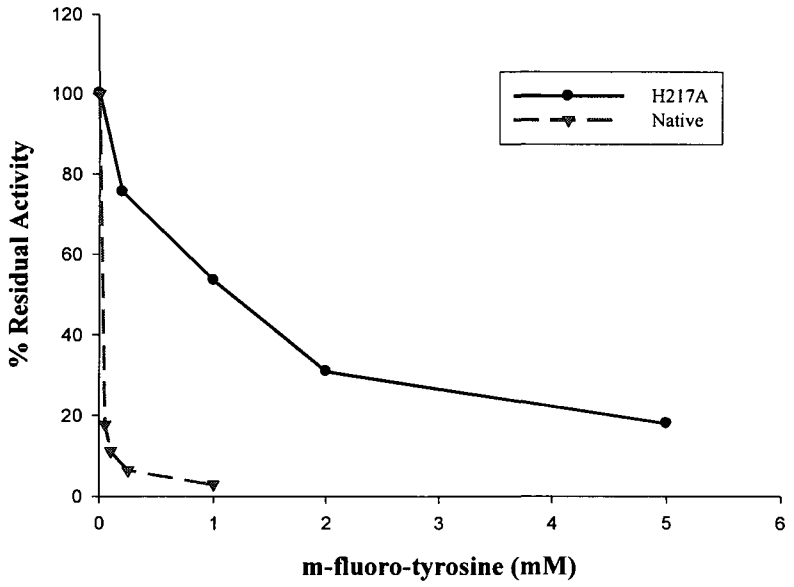

Figure 16: Effect of *m*-fluoro-DL-tyrosine on PD activity of native and H217A variant Δ19PDs

Assays were carried out at 55°C in the presence of *m*-fluro-tyrosine (0-5 mM) in reaction buffer containing 100 mM HEPES, 100 mM Tris and 150 mM NaCl, adjusted to pH 7.5 as indicated in section 2.17, and at a saturating concentration of NAD^+ (2 mM) and concentrations of prephenate of 0.35 mM (~ 4 x K_m) for native enzyme and 4 mM (~ K_m) for H217A. Estimated IC_{50} values for *m*-fluoro-DL-tyrosine at the substrate concentration given are 0.03 mM and 1 mM for native enzyme and H217A, respectively.

3.6 Thermal Stability Studies on Native Enzyme and H217A Variant

During the purification procedure, it was noted that H217A, unlike most other variants, precipitated readily when dialyzed against storage buffer. This feature combined with its low specific activity, greatly reduced catalytic efficiency and increased feedback resistance to tyrosine promoted us to determine if the change of His217 to alanine had destabilized the structure of this variant. We attempted to determine if H217A was more thermally labile than native Δ19PD by examining the loss of far-UV CD signal as a function of temperature. Changes in ellipticity at 222 nm were recorded from 25°C-95°C. As shown in Figure 17A, both proteins appeared very resistant to temperature-induced changes in global secondary structure. By 95°C, the native and variant enzymes had lost only 27% and 40%, respectively, of their ellipticities. Neither protein yielded denaturation curves indicating cooperative transitions within this temperature range, although the variant's change in ellipticity commenced immediately from the onset of the temperature ramp and continued steadily through to 95°C. Additionally, it appeared that by 95°C significantly more H217A than native enzyme had precipitated in the reaction cuvette. A full wavelength scan of native protein before and after the variable temperature scan (Figure 17B) revealed a signal change of ~ 30%. This likely correlated with a decrease in protein concentration rather than unfolding of native protein to soluble denatured sample. Overall, the data support the idea that H217A is somewhat less thermally stable than native enzyme.

The thermal stabilities of native and H217A variant Δ19PD were probed further by incubating the enzymes at 95°C for up to 23 h and recording PD activities at 55°C and protein content of aliquots removed at specific time points. Figure 18 shows the effect of

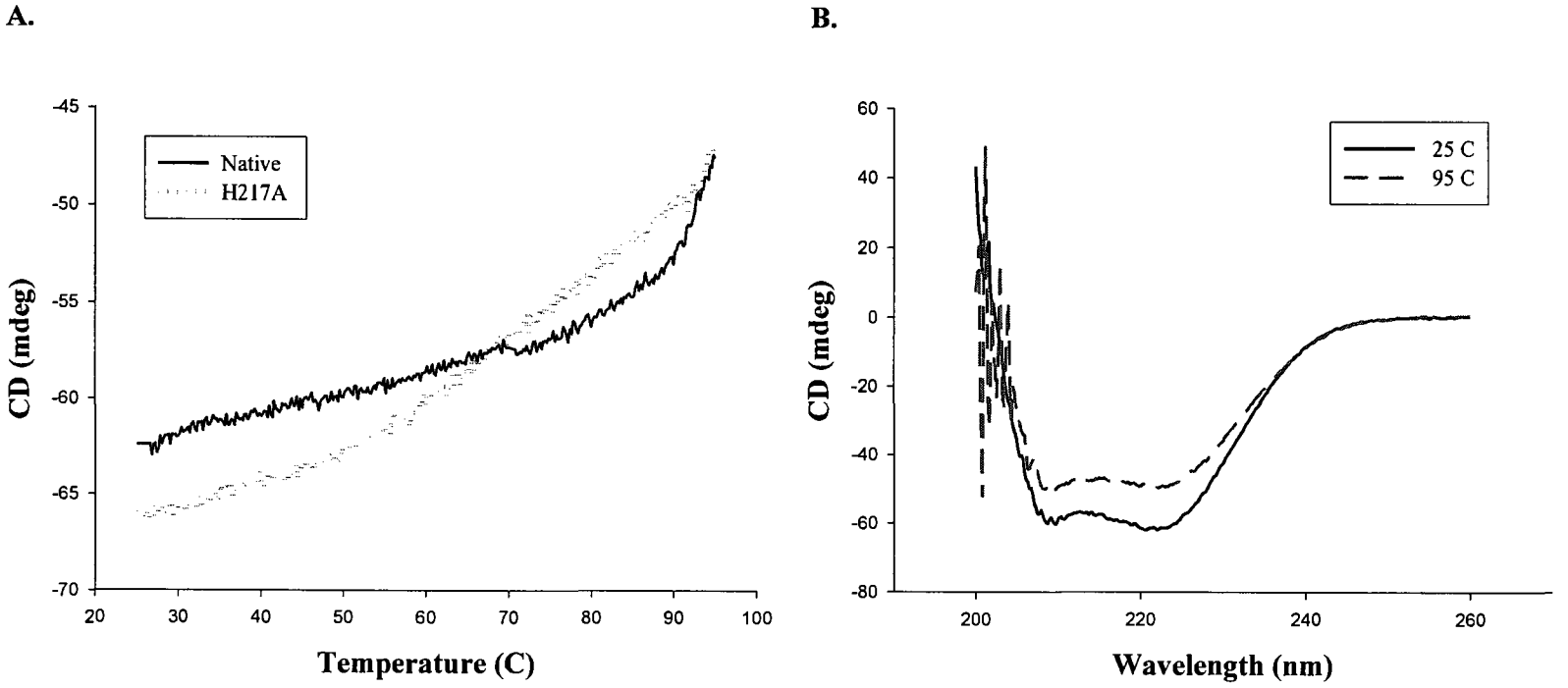

Figure 17: Variable temperature far-UV CD spectra of native and H217A Δ19PDs

Proteins (16.6 μM monomer) were in 50 mM potassium phosphate, 500 mM NaCl, pH 7.5. **(A):** Spectra were recorded at 222 nm in a 0.1 cm path-length rectangular cell from 25°C to 95°C, using a ramping speed of 40 °C/h. Variation in CD signal (3 mdeg, at 25°C) between native and H217A variant was likely due to the slight difference in protein concentration. **(B):** Far-UV CD spectra of native enzyme at 25°C and 95°C. Spectra represent the average of 5 accumulations recorded at a scan rate of 100 nm/min in a 0.1 cm path-length rectangular cell.

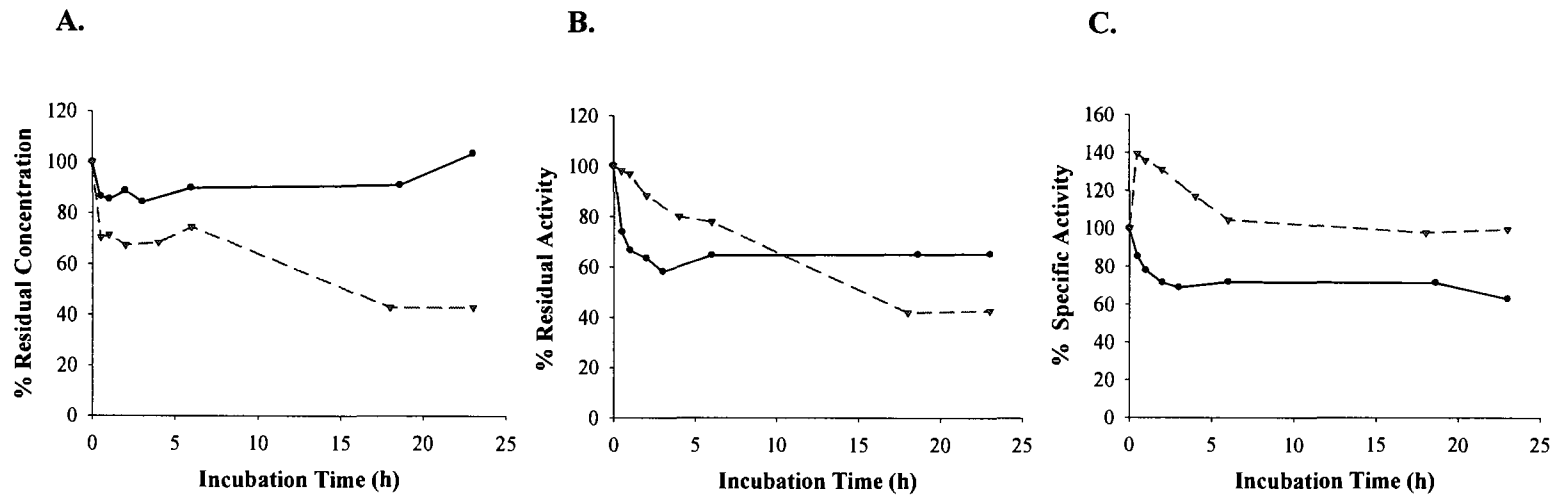

Figure 18: Thermal inactivation of native and H217A variant Δ19PDs

Native enzyme (0.9 mg/mL) and H217A variant (1 mg/mL) in a buffer of 50 mM HEPES/150 mM NaCl, (pH 7.5) were incubated in capped Eppendorf tubes at 95°C. At specific time intervals, tubes were removed, cooled on ice for 2 min, centrifuged at maximum speed for 5 min at room temperature. Protein concentrations of the samples were determined by using the Bio-Rad reagent and the residual PD activity were determined at 55 °C by the standard assay as outlined in section 2.12 using 5 μL of native enzyme or 80 μL of the H217A variant. The concentration of NAD^+ in the assay was fixed at 2 mM while prephenate was either 1 mM or 4 mM for native and H217A, respectively. Measurements were performed as a ratio of the parameter in a specific incubation time relative to t = 0. Solid line: native enzyme; Dashed line: H217A. Incubation time was plotted as a function of **(A)** residual protein concentration, **(B)** residual activities and **(C)** residual specific activities.

temperature on protein concentration (A), enzyme activity (B) and specific activity (C). Consistent with the results from the variable temperature far-UV CD experiments, the concentration of soluble H217A protein (Panel A) dropped significantly more with increased incubation time than did native enzyme. Surprisingly, however, this did not correlate with the much slower time-dependent reduction in PD activity observed for the variant (Panel B). Consequently, the residual specific activity of H217A increased before decreasing slowly then levelling off (Panel C). It is clear that both proteins regain partial to full enzyme activity once they are removed from the high temperature incubation and are assayed at 55°C. Interestingly, our results differed from that of Bonvin *et al.* (*50*) who reported a half life at 95°C of ~ 1 h for Δ19PD, even though the experimental set up in this study was identical to that reported by Bonvin. Different incubation conditions were tested (buffers with higher salt, glycerol, or Tris) yielding variable results, so experiments were not pursued further at this time. Overall, the data indicated that under these experiments conditions, both proteins were resistant to thermally-induced inactivation.

Bonvin *et al.* (*50*) indicated that dimeric native Δ19PD undergoes oligomerization during its Gdn-HCl-induced pathway of unfolding. To determine if changes in quaternary structure also accompanied thermal denaturation, native PAGE was performed on native and H217A variant Δ19PD proteins after their incubation at 95°C from 0 to 3 h. As shown in Figure 19, at all time points both proteins migrated to a position in the gel corresponding to a mass of ~ 240 kDa (an octamer). Under non-denaturing conditions however, proteins will migrate through a polyacrylamide gel as a function of their charge as well as molecular weight. Since the isoelectric point of Δ19PD is high (7.78) due to a high proportion of basic enzymic residues, migration patterns of the protein in the gel

may not reflect their actual native molecular weight. Thus, size exclusion chromatography experiments must be performed in order to draw any definite conclusions concerning the quaternary structure of Δ19PD in this experiment.

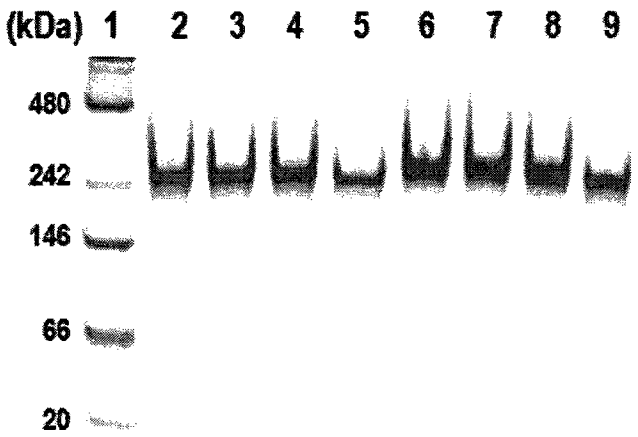

Figure 19: Non-denaturing PAGE analysis of native and H217A Δ19PDs

Protein samples analyzed were those used to generate the data shown in Figure 20 for incubation time at 95°C of 0 min, 30 min, 1 h and 3 h. Lane 1: Protein Standard, Lanes 2-5: native protein incubated at 95°C for 0 min, 30 min, 1 h and 3 h, respectively, Lanes 6-9: H217A protein incubated at 95°C for 0 min, 30 min, 1 h and 3 h, respectively. Electrophoretic analysis on a 7.5% polyacrylamid gel was performed under non-denaturing conditions as described in section 2.10. NativeMark™ Unstained Protein Standard (Invitrogen) was composed of apoferritin band1, B-phycoerythrin, lactate dehydrogenase, bovine serum albumin and soybean trypsin inhibitor, listed from top to the bottom.

3.7 The Effect of Gdn-HCl on Native and H217A Δ19PDs

The stabilities of native and H217A enzymes were compared by monitoring their resistance to Gdn-HCl-induced unfolding. Changes in the far-UV CD signal at 222 nm and in tryptophan fluorescence served as probes for the perturbation of secondary and tertiary structure, respectively. Proteins were incubated for 20 h at different concentrations of Gdn-HCl at room temperature as outlined by Bonvin *et al.* (*50*) to ensure that equilibrium measurements were recorded. Figure 20, Panel A illustrates the loss of CD signal at 6 M Gdn-HCl for H217A while Panel B shows the Gdn-HCl-induced changes in tryptophan fluorescence emission. In the absence of Gdn-HCl, maxima are observed at 317 and 330 nm, which are characteristic of tryptophan residues in a non-polar environment. By 1.5 M Gdn-HCl the tryptophan fluorescence intensity decreased. By 5.5 and 6 M Gdn-HCl the maximum emission wavelength shifts to ~ 342 nm and 355 nm, as the fluorophores became exposed to solvent. Interestingly, there were no shifts in λ_{em} maxima upon denaturation until the Gdn-HCl concentration reached 5.5 M. In Figure 21 the Gdn-HCl-induced changes in the CD signal at 222 nm and in tryptophan fluorescence intensity at a maximum emission wavelength of 317 nm were plotted together as percent fraction folded versus denaturant concentrations. Remarkably, both proteins appear quite resistant to chemical denaturation achieving less than 10% folded structure only by 6 M Gdn-HCl. However, the native and H217A variant proteins did not yield identical patterns of unfolding suggesting the variant was less stable. The Gdn-HCl denaturation plots were complex. The variant appeared to lose its tertiary structure more rapidly than the native enzyme. Additionally, the variant lost a significant amount of its tertiary structure before losing its secondary structure. Finally, in contrast to the native

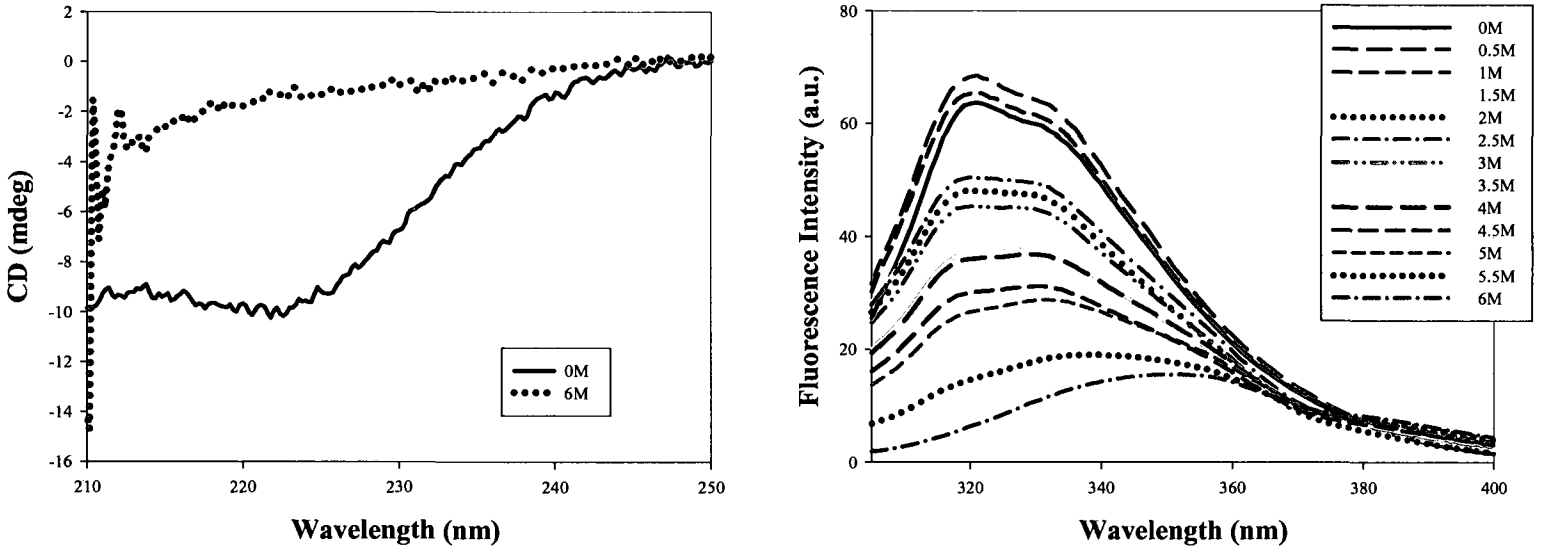

Figure 1: Select far-UV CD spectra (A) and fluorescence emission spectra (B) of H217A Δ19PD during Gdn-HCl-induced unfolding

Proteins (3μM monomer) were incubated in a buffer of 50 mM potassium phosphate, 75 mM NaCl, pH 7.5, at room temperature in the presence of different concentrations of Gdn-HCl for 20 h. The fluorescence emission spectra were recorded at an excitation wavelength of 295 nm using excitation and emission bandwidth of 4 nm and far-UV CD spectra were recorded from 250 nm to 210 nm. The fluorescence emission spectra and far-UV CD spectra were performed as described in section 2.14 and 2.13, respectively.

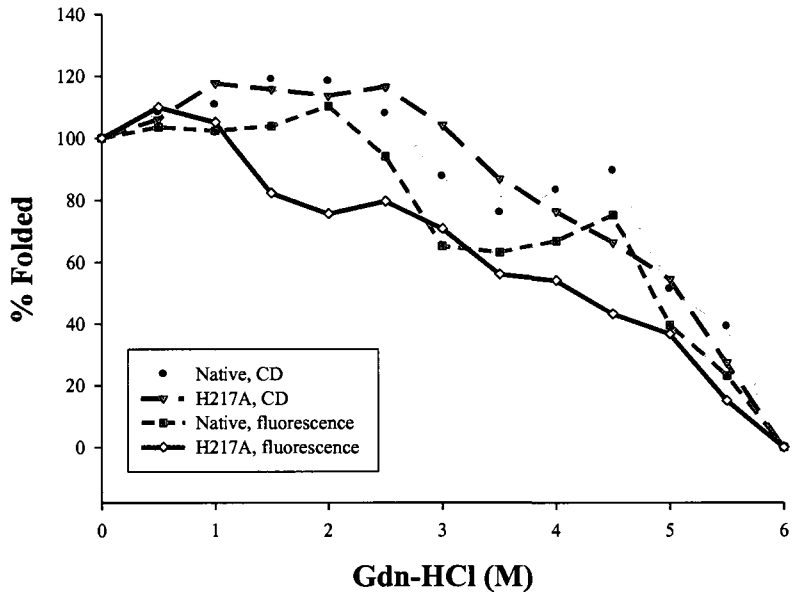

Figure 21: The effect of Gdn-HCl on intrinsic fluorescence and CD ellipticities of native and H217A Δ19PDs

The fraction of folded protein was plotted as a function of Gdn-HCl concentration using a signal change at 222 nm or maximal fluorescence emission intensity of 317 nm at λ_{ex} 295 nm. Protein (3 μM monomer) was in a buffer containing 50 mM potassium phosphate and 75 mM NaCl, pH 7.5 (PPS). Percent folded at each concentration of denaturant was calculated as described in section 2.14.

enzyme, the variant's fluorescence and CD spectra did not exhibit a plateau which represents a stable intermediate species formed during the unfolding pathway between 3-4.5 M Gdn-HCl .

Further evidence that there is a difference in the chemical stability and/or active site structure of the variant as compared to the native enzyme is shown in Table 8. Low concentrations of Gdn-HCl activate PD activity of the native enzyme but cause inactivation of H217A.

Table 8: The effect of low concentrations of Gdn-HCl on PD activity

Gdn-HCl (M)	% Activity in absence of Gdn-HCl	
	Native	H217A
0	100	100
0.5	170	28
1	102	7

Δ19PD proteins (10 μg of native enzyme and 240 μg of H217A in PPS buffer) were pre-incubated for 2 min at 30°C in reaction buffer containing different concentrations of Gdn-HCl. Enzyme activities were recorded after the addition of NAD^+ (2 mM) and prephenate (1 mM for native enzyme and 4 mM for H217A)

Chapter 4: Discussion

The purpose of this thesis was to examine the functional and structural importance of selected residues in the reaction catalyzed by a monofunctional prephenate dehydrogenase from the extreme thermophile *Aquifex aeolicus*. Specifically, attempts were made to assign roles for the active site residues Lys246', Arg250, and His217 in substrate binding and catalysis, and in the inhibition by the end product L-tyrosine. One residue Trp190 was selected to further decipher its contribution to the fluorescent properties of the enzyme. We have correlated these results with several crystal structures available for the enzyme bound with NAD^+ alone and in complex with HPP or L-tyrosine or modeled with prephenate, and when applicable, we have compared them with results from site-directed mutagenesis on *E. coli* CM-PD. Sequence alignments of *A. aeolicus* PD with other bacteria and yeast TyrA proteins (Figure 5) reveal that Arg250, His217 and Lys246' appear well conserved. A battery of variant proteins were expressed and purified; in some examples a signal replacement was made (H217A, W190F) while in other cases a multiple substitutions at a single position were studied (R250Q/A/K, K246Q/A).

Modifications were made to a protocol that had been devised initially for crystallographic high-throughput protein purification (*40*) in order to circumvent problems stemming from low protein expression (as seen with W190F) and/or poor specific activities and proteolysis (with R250Q) (Table 4). Collectively, the revisions resulted in a 4 to 20-fold increases in Δ19PD protein from just 0.5 L of culture—one-eighth the culture volume routinely processed when using the original protocol. Four steps that likely contributed the greatest to improvements in expression and purification

included 1) re-circulating the cell-free extract through the affinity column for efficient protein binding, 2) thorough column washing prior to eluting PD protein with 300 mM imidazole, 3) lysing cells with BugBuster™ protein extraction reagent instead of with pressure and sonication, and 4) culturing in Overnight Express Instant™ TB medium at 37°C which is reported to promote very high cell density growth. Additionally, transforming mutant plasmid into BL21(DE3)pLysS can also help the protein extraction since plasmid pLysS encodes the T7 lysozyme which, in addition to inhibiting T7 RNA polymerase until IPTG is added, can also hydrolyse the *N*-acetylmuramide linkages in the peptidoglycan layer of the cell wall.

All variants were routinely obtained in good yields (Table 5) when following the revised protocol, and could be purified to homogeneity as determined by SDS-PAGE (Figure 10) and mass spectrometric analysis (Figure 11). The kinetic parameters of native and H217A Δ19PD proteins purified by either method are in excellent agreement with those that have been previously reported by Bonvin and coworkers in our lab (*50*).

Global structural features and the assignment of W190's contributions to fluorescence.

Analysis of Far-UV CD spectra (Figure 12) indicated that at room temperature the global secondary structure of the variants had not been altered as a result of the substitutions. The spectra showed in all cases a double minimum at 208 and 222 nm, which is in agreement with the high level of α helical structure (47%) calculated from crystallographic data which is represented in Figure 6. The structure also reveals that

much of the helical content of the protein stems from the extensive C-terminal dimerization domain.

Similarly, a comparison of the fluorescence intensity of all variants except W190F indicated that the environment surrounding the proteins' two tryptophan and ten tyrosine residues were not perturbed by the amino acid replacements (Figure 13). Furthermore, the analysis of W190F allowed dissection of the contribution of each of the two tryptophan groups/monomer to the overall fluorescence emission of the protein. Although the native Δ19PD exhibited two emission maxima, one at 317 nm and one at 330 nm, the peak at 317 nm was eliminated by the conversion of Trp190 to phenylalanine, leaving a single emission maximum at 330 nm. Thus, the peak at 317 nm and 330 nm must be due to Trp190 and Trp259, respectively. Moreover, both tryptophan groups contributed equally to the global fluorescence emission of the protein since the emission intensity of W190F from excitation at either at 280 nm or 295 nm was approximately one-half that of the native enzyme. Both tryptophan groups were buried but notably Trp190, as deduced from the peak maixma which were considerably blue shifted to that predicted for a solvent exposed Trp (355 nm). These findings are in agreement with the crystal structure of the NAD^+-bound enzyme which places Trp190 on helix 7, its side chain completely buried within the hydrophobic core of the Rossman fold of the NAD^+ binding domain, which is near to but not in the active site (*40, 50*). In contrast Trp259 lays partially buried on helix 11 within the prephenate binding pocket (Figure 22). The space filling model (Figure 23) illustrates the degree of solvent accessibility of these two tryptophan groups. The results support the findings of Bonvin *et al* who showed that the fluorescence emission

equivalent to one of the two tryptophan residues could not be eliminated by the external quenching agents, acrylamide and KI (*50*).

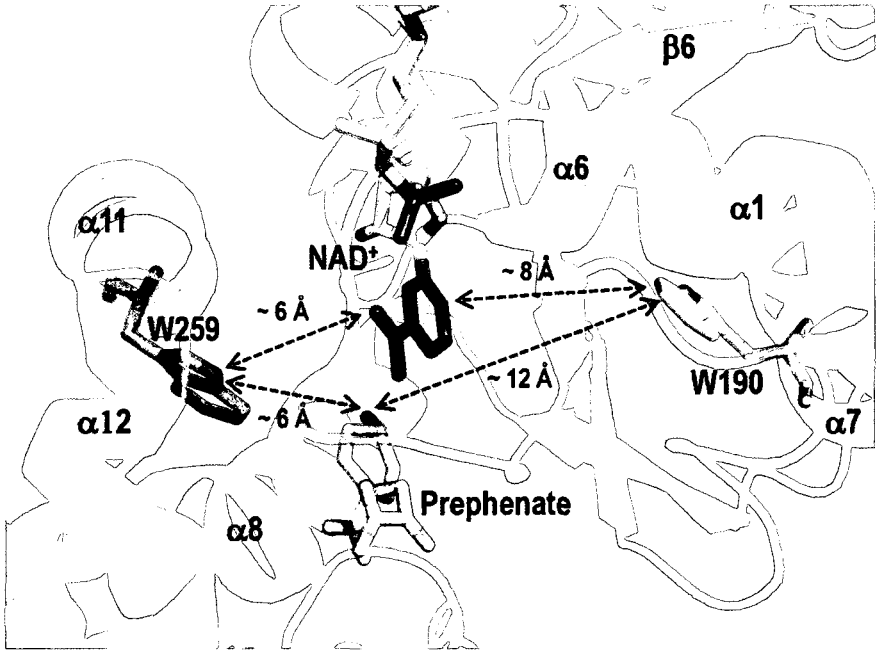

Figure 22: Structural relationship between tryptophan residues and the substrates, prephenate and NAD^+

Both tryptophan groups are in close proximity to both substrates (prephenate is modeled in the active site). The indole nitrogen of Trp259 is partially buried in the inter-domain cleft and is ~ 6 Å away from the C-4 hydroxyl group of prephenate and the nicotinamide ring of NAD^+. The side chain of Trp190 is buried in the N-terminal NAD^+ binding domain and is ~ 8 Å and 12 Å from the nicotinamide ring of NAD^+ and the pyruvyl side chain of prephenate, respectively. Picture generated using PyMOL (*46*) using the coordinates in reference (*40*).

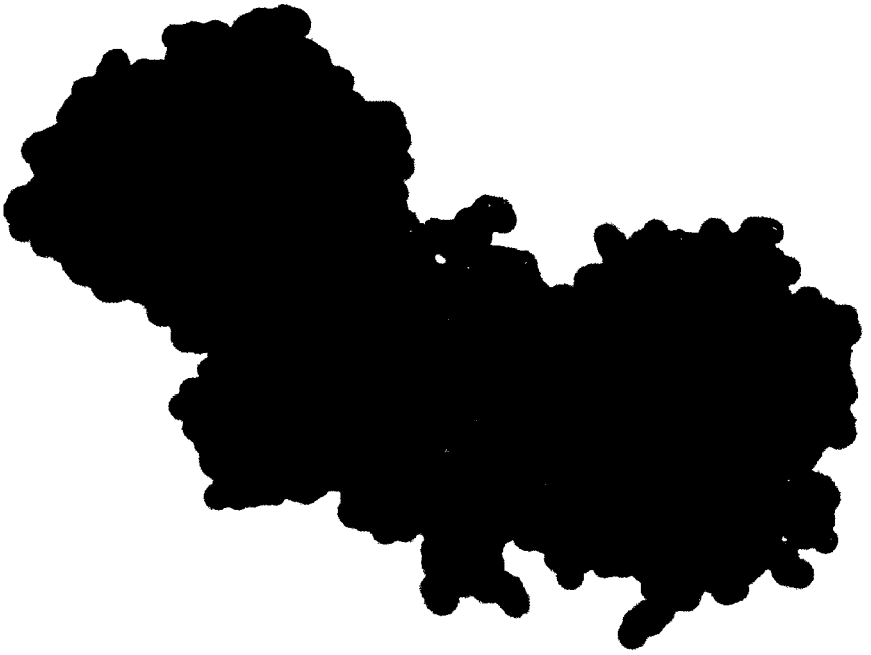

Figure 23: Space-filling model of dimeric *A. aeolicus* Δ19PD

One subunit is colored in green, the other one is in red. Trp190 and Trp259 from each subunit are colored yellow and blue, respectively. This model was generated using PyMOL (*46*) using the coordinates given in reference (*40*).

Arg250 is important but not critical for prephenate binding

The recently acquired crystal structure of the enzyme liganded with NAD^+ and HPP at neutral pH (*41*) shows that Arg250's guanidinium group forms two ion pairs (< 3 Å) with the side chain carboxyl groups of the product (see Figure 24). Moreover, Arg250 also appears locked in place aided by an ionic network involving the negatively charged side chain oxygens of Glu153 and Asp247'. Accordingly, Arg250 is ordered and shows excellent electron density, in contrast to what was observed in the structure determined at pH 3.2 without HPP bound (*41*).

Given the number of important interactions which are structurally dependent on Arg250, it is surprising then that the glutamine substitution (R250Q) causes only a 13-fold reduction in prephenate binding, and remarkably, a similar change is also seen for the alanine replacement—a side chain which is unable to participate in electrostatic interactions. The cationic group and/or side chain length is clearly important however, as the lysine variant increased the binding of prephenate by 4-fold relative to the alanine variant. No changes in the K_m for NAD^+ or catalytic turnover number were observed revealing the importance of this group's interaction with prephenate only.

The results of this kinetics study are contrary to that reported for *E. coli* CM-PD, where changes in the homologous residue, Arg294, with a glutamine resulted in an over 120-fold decrease in prephenate binding (*31*). This change in binding affinity highlights the importance of the arginine residue in prephenate binding in the *E. coli* enzyme and also suggests that there are differences in the active site geometry between the two dehydrogenases.

A.

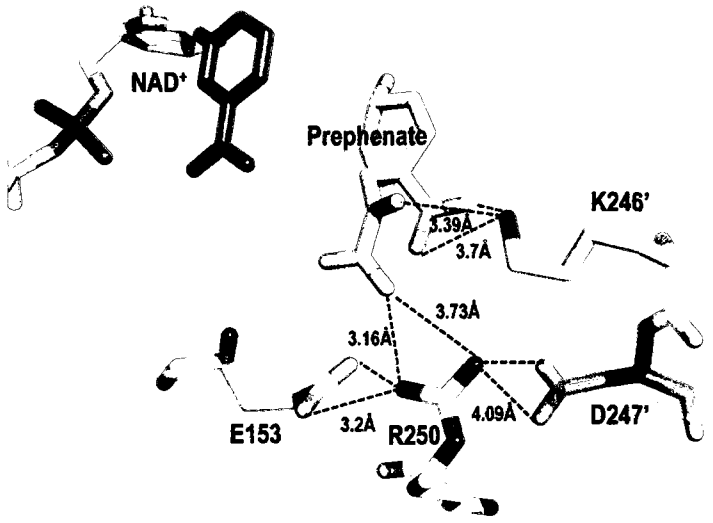

B.

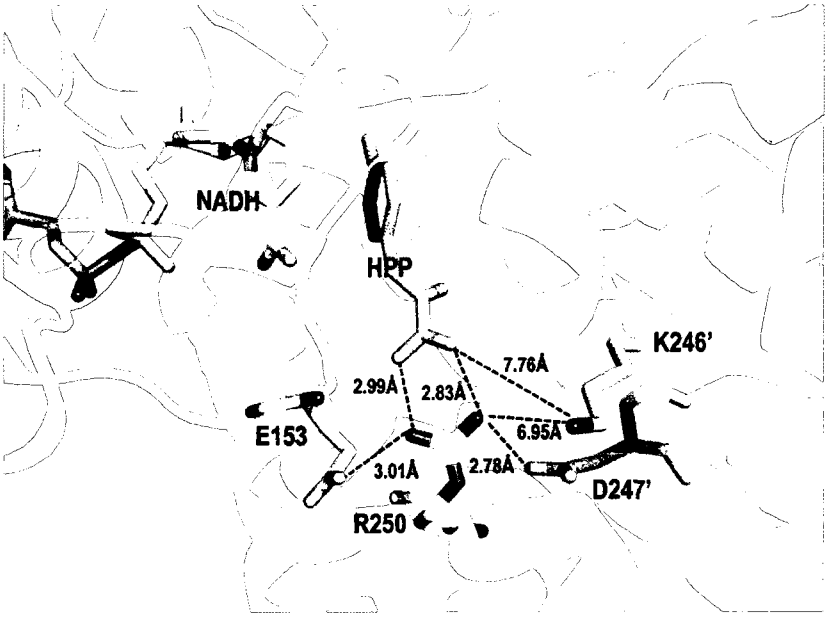

Figure 24: Crystal structure of dimeric Δ19PD showing important inter-subunit interactions

The crystal structure of Δ19PD-NAD^+ complex was solved at pH 3.2 for the enzyme liganded with NAD^+ and with prephenate modeled in the active site (A) and at pH 7.5 in complex with NADH and HPP (B). The access of prephenate is mediated by a "gate" composed of E153-R250-D247'. Note: in (A) Lys246' is directed toward prephenate while in (B) Lys246' is pointing away from HPP. Pictures created using PyMOL (*46*) using the coordinates given in references (*40*) and (*41*), respectively.

The magnitude of the loss of apparent binding affinity of R250Q/A for prephenate (~1.5 kcal/ mol) is more in keeping with the elimination of a H-bond rather than a strong ionic interaction; thus, this guanidinium group is not an essential binding residue. It may be that residues other than Arg250 also contribute to the positioning of prephenate in the active site and their roles may have greater impact in the Ala/Gln variants. For example, a bound water molecule (WAT2) is shown in the HPP liganded structure (Figure 25) to be 2.66 Å from the side chain carboxylate oxygen of HPP and held in place through a H-bond with His217 and Ser254 (*41*). Additionally, mutagenesis analysis by Bonvin shows that Ser126 is important for prephenate binding. The K_m for prephenate increases 10-fold and k_{cat} decreases 10-fold in the S126A variant. The crystal structure reveals that the 4-hydroxyl group of HPP is positioned through a H-bonding network involving Ser126, His147 (the catalytic H-bond acceptor) and another bond water molecule (WAT1).

Mutagenesis experiments in AD from *Synechocystis* sp. might provide additional comparisons. Legrand *et al.* (*33*) have proposed that the equivalent residue to Arg250 in this TyrA protein (Arg217 in AD) is too far away from the active site pocket to interact directly with arogenate. Christendat and coworkers showed however, by overlaying the structure of AD with *A. aeolicus* Δ19PD liganded with NADH and HPP, that Arg217 may indeed interact with the product (*41*).

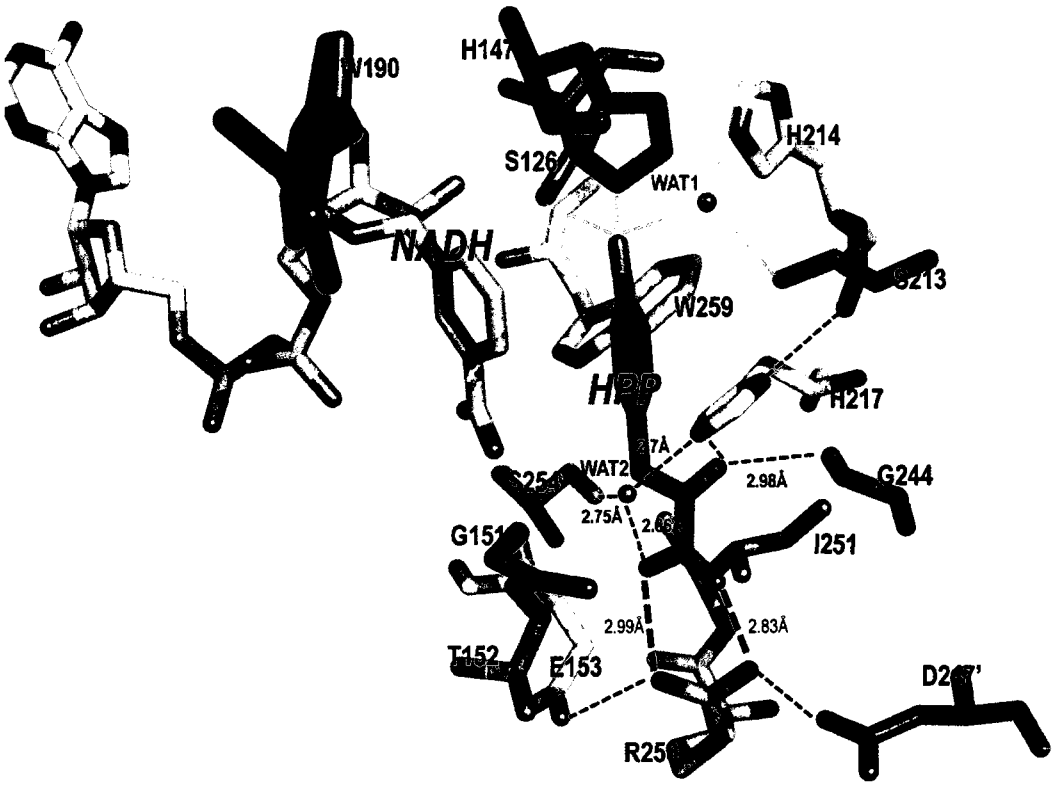

Figure 25: Active site of *A. aeolicus* Δ19PD in complex with NADH and HPP at pH 7.5

R250 interacts directly with the side chain carboxylate group of HPP (shown in black dashed line), and is positioned through ionic interactions with the side chains of E153 on the same monomer and D247' on the adjacent monomer. Another important ionic network binding involves HPP, S254, WAT2 and H217 (highlighted in blue). The 4-hydroxyl group of HPP is coordinated with a H-bonding network consists of S126, H147, WAT1 H214 and S213 (shown in grey dashed line). WAT = water. Picture created using PyMOL (*46*) using the coordinates given in reference (*41*).

Lys246's role in prephenate binding is not precisely determined

As noted with Arg250, the kinetic results shown in Table 7 also indicate that Lys246' participates solely in the binding of prephenate and not in the enzyme's interactions with NAD^+ or in catalysis. Moreover, electrostatic interactions are important as the alanine variant reduced prephenate binding by over 20-fold whereas the glutamine substitution caused only a 5-fold reduction in binding. In contrast, the equivalent mutation in *E. coli* CM-PD (R286A) caused less than a 2-fold increase in K_m for prephenate (*31*), again indicating that the active site environment of *A. aeolicus* Δ19PD may be different than in *E. coli* CM-PD.

Our kinetic data support more closely the finding of the crystal structure of *A. aeolicus* Δ19PD complexed with NAD^+ at pH 3.2 where it is revealed that Lys246' from the adjacent monomer is in close proximity to the ring carboxylate group and the pyruvyl side chain of prephenate molecule that has been modeled in the active site (Figure 24, Panel A). In contrast, the structure determined at pH 7.5 in the enzyme-NADH-HPP complex shows that the identical lysine group oriented away from the active site and making no directed interactions with HPP or with other nearby acidic residues, such as Glu153 and Asp247', both of which have been proposed to participate along with Arg250 in a gated mechanism that modulates prephenate's entry into the active site (*40*). It might be that Lys246's role is also to help to guide negatively charged prephenate towards the active site assisted by Arg250 and Arg307. Such a mechanism has been proposed for a cationic cluster involving Arg213, Arg217, Arg274', Lys202 and Lys276' in AD of *Synechocystis* sp. (The first three residues are equivalent to Lys246', Arg250 and Arg307 in *A. aeolicus* Δ19PD).

We have commenced chemical and mass spectrometry studies to probe Lys246's surface accessibilities in the presence and absence of substrates. Further refinement of the role of Lys246 in prephenate binding would benefit by modeling prephenate into the active site of the enzyme-NAD^+ complex at pH 7.5 and by performing inhibition studies in the presence of prephenate and HPP and its analogues as steps towards defining the importance of the ring carboxyl group in placing prephenate in the active site.

His217 is important for maintaining the integrity of the active site

The results from our kinetic studies show striking differences in the kinetic parameters for the reaction catalyzed by H217A compared to the native enzyme. The efficiency constant of the variant is reduced by over three orders of magnitude, reflecting large changes in both prephenate binding and catalysis (Table 7). This effect may be due to a loss of direct electrostatic interactions with residues that coordinate prephenate or through global structural perturbations in the active site. Surprisingly, the fluorescence emission spectrum of H217A was not perturbed compared to that of the native protein (Figure 13) as the imidazole ring of H217 is stacked against the indole ring of Trp259 in the active site. The crystal structure of the enzyme with HPP shows that His217 has no direct interactions with prephenate; instead the main chain amide group of Gly244 can directly H-bond to the keto group of the propionyl side chain. However, the Nε-2 group of His217's imidazole ring is coordinated to a bound water molecule (WAT2) which makes important interactions through a H-bonding network with several groups: the side chain hydroxyl of Ser254, the guanidinium group of Arg250 and the keto and carboxyl groups of the ligand (see Figure 25). Thus, the conversion of His217 to alanine would

certainly have adverse effects on prephenate binding. The observation that k_{cat} is greatly affected indicates that this substitution can alter the catalytically competent form of the enzyme. As shown in Figure 25, the Nδ1 group of His217 also H-bonds to the mainchain carbonyl group of Ser213. Since Ser213 is linked to an important electrostatic network involving His147 (a key participant in the hydride transfer reaction), the H217A variant could indeed affect catalysis. Interestingly, Bonvin noted that an asparagine substitution also yielded similar results to that of H217A. Thus, these important electrostatic interactions appear to be only satisfied by an imidazole ring.

Studies by the Turnbull lab have indicated that the H257A variant in *E. coli* CM-PD (equivalent to H217A in *A. aeolicus* Δ19PD) results in only small changes in catalytic efficiency of the dehydrogenase (*30*). Moreover, the active site residue Trp259 is not conserved (it is replaced with a tyrosine in *E. coli* CM-PD and in *H. influenza* PD, Figure 5). Therefore, variations in the corresponding amino acids may explain varying levels of perturbation in the kinetic properties between H217A and H257A proteins from *A. aeolicus* PD and *E. coli* CM-PD.

The structure depicted in Figure 25 shows that Ile251 and Trp259 participate in hydrophobic stacking with His217; the loss of this interaction could greatly perturb the structure of the active site and in turn, significantly alter the kinetic parameters of the reaction. The following observations are consistent with this idea:

(1) Concentrations of Gdn-HCl (0.5, 1 M), which normally activate native Δ19PD enzyme at room temperature (Table 8, (*50*)) presumably through loosening of its rigid structure, are shown to greatly reduce the activity of His217A. This loss of activity is accompanied by a slight increase in fluorescence intensity, as would be expected if

perturbations in the active site move Trp259 away from quenching agents such as the protonated imidazole groups of His217 and His214.

(2) The denaturation profile in Figure 21 shows that with increasing concentrations of Gdn-HCl, His217A loses tertiary structure more rapidly and to a larger extent than does the native enzyme. Additionally, the amino acid change appears to eliminate a plateau between 3-4.5 M denaturant which Bonvin *et al.* (*50*) attributes to an oligomeric intermediate in the unfolding pathway deduced for the native Δ19PD enzyme.

(3) His217A was also more labile during protein purification and somewhat during temperature unfolding. Thermal denaturation more readily accompanied protein precipitation by the variant enzyme as determined through protein assays from samples heated at 95°C (Figure 18A), or slowly through changes in CD signal when the temperature is increased step-wise (Figure 17). It is worth noting that Aponte (*61*) and Bonvin *et al.* (*50*) have previously reported that *A. aeolicus* PD is very resistant to temperature-induced changes in protein secondary structure as deduced through variable temperature-Fourier transform infrared spectroscopy studies and that the protein can regain secondary structure upon cooling.

Histidine plays a role in tyrosine inhibition

Results from recent crystallographic studies and kinetic inhibition data show that both the immediate product (HPP) and the end product (L-tyrosine) bind to the active site of native Δ19PD from *A. aeolicus* and compete directly with prephenate for this binding pocket. Moreover, HPP and L-tyrosine bind to the active site with affinity that is

comparable to that of prephenate (*41*). Accordingly, since the H217A variant cannot bind prephenate well (Table 7), it follows that it will no longer retain its interactions with L-tyrosine. Our results examining the loss of PD activity with increasing tyrosine concentrations are in agreement with this; H217A is not inhibited by L-tyrosine even at 7.5 mM, a concentration which eliminates 95% of native Δ19PD activity. Only in the presence of 5 mM *m*-DL-fluorotyrosine (a tight-binding tyrosine analogue), do we see significant inhibition of PD activity of H217A (Figure 16). Thus, Δ19PD from *A. aeolicus* joins the list of other two TyrA proteins (i.e. *E. coli* CM-PD (*12*) and AD from *Nicotiana silvestris (28)*) that are reported to be very sensitive to the effects of the fluorinated tyrosine analogue.

Comparison of the crystal structure of Δ19PD in complex with HPP (Figure 25) and L-tyrosine (Figure 26) show that the amino group of tyrosine (unlike the keto group of HPP) is pointing away from His217 and toward the main chain carbonyl group of Thr152 and WAT2. However, many of the other electrostatic interactions which hold HPP in the active site are also important for positioning L-tyrosine.

In accordance with the crystal structures, the decrease in prephenate binding by R250A (Table 7) also correlates with the poorer inhibition by L-tyrosine (Figure 15). In agreement, the R250Q/A variants are less inhibited by L-tyrosine than is the lysine variant. Some of the same interactions that hold prephenate in the active site also retain L-tyrosine; Arg250's guanidinium group is coordinated to the side chain carboxylate group of L-tyrosine and of HPP. Surprisingly, this correlation does not hold for the K246A/Q variants which are more inhibited by L-tyrosine yet possess higher K_m values for prephenate. Additionally, the W190F variant is moderately feedback resistant to

tyrosine although it possesses kinetic parameters similar to that of the native enzyme. Thermodynamic studies examining tyrosine binding in the absence of prephenate must be completed to more accurately define the relative contributions of the different active site residues.

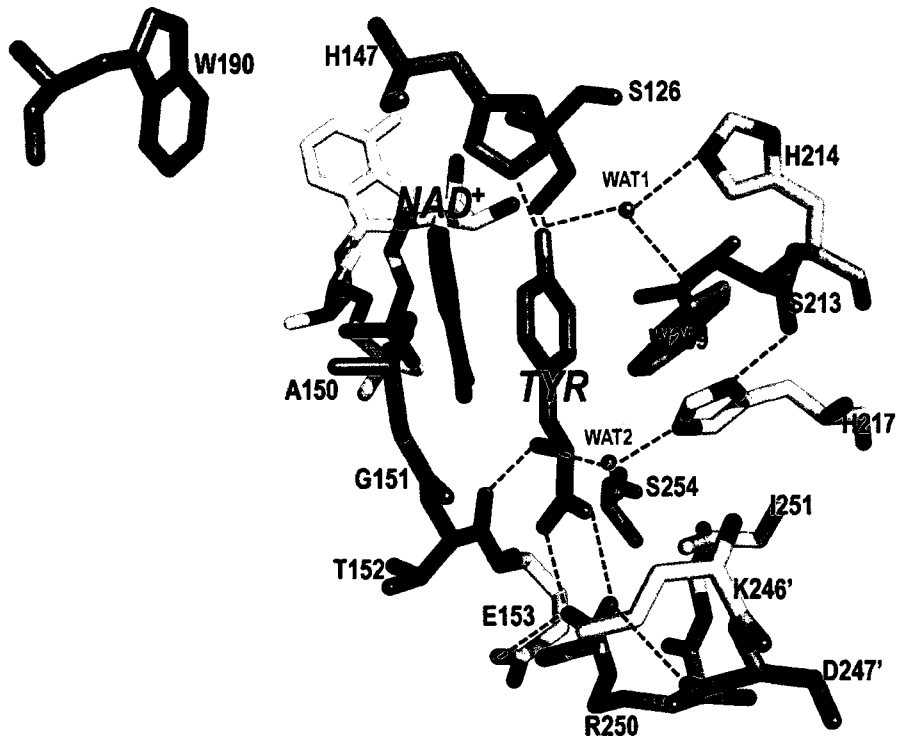

Figure 26: Crystal structure of *A. aeolicus* Δ19PD complexed with NAD^+ and L-tyrosine at pH 7.5
"TYR" refers to L-tyrosine while "WAT" refers to water. Primed residues represent residues from the other subunit of the dimeric enzyme. Note that the amino group of the ligand L-tyrosine is pointing away from His217 and interacts with the main chain carbonyl group of Thr152 and WAT2. Picture created using PyMOL (*46*) using the coordinates given in reference (*41*).

Christendat and Turnbull and their coworkers (*41*) have speculated that the altered binding mode of L-tyrosine versus HPP is due to a protonated His217 which produces an electrostatic repulsive effect and directs the interaction of the protonated amino group of tyrosine away from this histidine and towards the backbone carbonyl group of Thr152. If this is the case, then one would predict that the fluorescence emission of native enzyme contributed by Trp259 might be quenched due to tryptophan's proximity to a protonated side chain (i.e., the imidazole of His217). Our result comparing the fluorescence emission of native Δ19PD and H217A variant (Figure 13) do not support this hypothesis; perhaps a comparison of the fluorescent properties of the double mutant W190F/H217A with that of W190F might show the changes in fluorescence quenching that are predicted.

It is worth noting that L-tyrosine likely interacts at the HPP binding site (and by inference, the prephenate site) of TyrA from *H. influenza* as noted for *A. aeolicus* Δ19PD. Nevertheless, the binding mode of L-tyrosine to PD from *H. influenza* appears to be distinct from that found in the *A. aeolicus* enzyme, based on the available crystal structures of the tyrosine-liganded PDs from the two organisms (Figure 26 and 27). As shown in Figure 27 two enzymatic tyrosine residues (Tyr288' and Try306) in the active site of *H. influenza* PD help coordinate the ligand's amino group but are absent in Δ19PD from *A. aeolicus*. Interestingly, His260 (equivalent to His217 in Δ19PD from *A. aeolicus* and His257 in *E. coli* CM-PD) is H-bonded to Tyr288'. Mutagenesis and binding studies are currently underway to test the model of tyrosine inhibition in the TyrA proteins from *H. influenza* and its homologous TyrA protein in *E. coli* CM-PD.

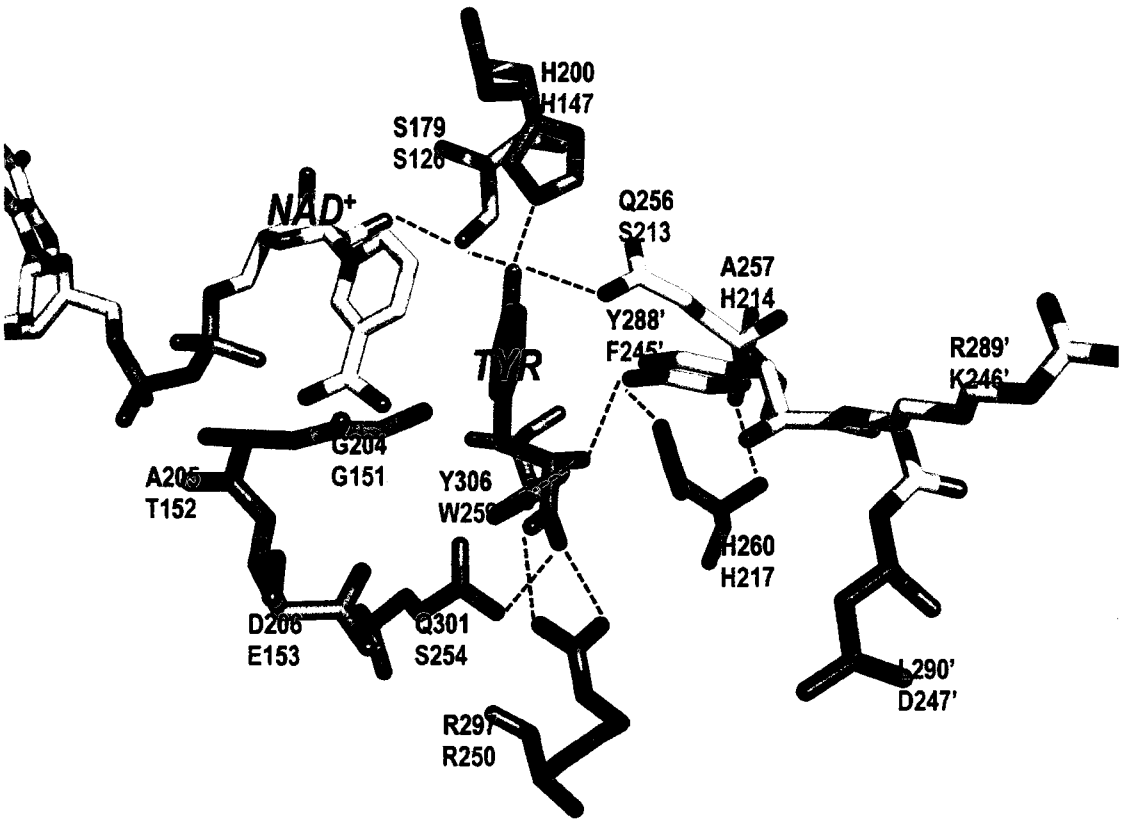

Figure 27: Active site of *H. influenzae* PD in complex with NAD^+ and L-tyrosine

The crystallisable form of TyrA from *H. influenza* is a Δ81enginieered variant with the removal of the first 81 amino acids of the 100 residue CM domain. Coordinates of the unpublished crystal structure are provided in PDB: 2PV7 and are used to generate this diagram. All dotted lines refer to H-bonding distance less than 3 Å. Labels in black refer to amino acid residues in *H. influenza* PD while those in red refer to the equivalent residues in *A. aeolicus* Δ19PD.

Chapter 5

Summary and Future Work:

Seven variant proteins W190F, H217A, K246A/Q and R250A/Q/K were characterized to provide insights into their importance in the mechanism of the reaction catalyzed by the hyperthermophilic prephenate dehydrogenase from *A. aeolicus*. Site-directed mutagenesis was successfully performed to generate the desired mutations within Δ19PD plasmid DNA. Proteins were then over-expressed and purified to homogeneity with excellent yields by following a revised procedure employing affinity chromatography. Determination of kinetics parameters of the reaction catalyzed by the variants revealed that Arg250 and Lys246' are important for prephenate binding while His217 is critical for both prephenate binding and catalysis. The secondary and tertiary structures of the variants were not perturbed by the amino acid replacements as judged by fluorescence and Far-UV CD spectroscopic analysis except for W190F whose tryptophan fluorescence emission revealed that Trp190 resides in a fully buried location within the protein in contrast to Trp259. Chemical and thermal stabilities of H217A were reduced compared to the native enzyme indicating that a histidine at position 217 was likely essential for the structural integrity of the active site. All variants showed altered sensitivity to inhibition by L-tyrosine but most notably, H217A which was the most feedback resistant. Our results were interpreted in term of the overall crystal structure for *A. aeolicus* Δ19PD and for other TyrA proteins.

Further site-directed mutagenesis studies will probe the effects of additional active site residues involved in tyrosine binding and substrate specificity. The crystal structure of *A. aeolicus* Δ19PD complexed with NAD^+ and L-tyrosine, at pH 7.5 (*41*) clearly

shows that L-tyrosine binds in the active site by interacting with the main chain carbonyl group of Thr152. Therefore, the conversion of Thr152 residue to a proline or an alanine residue should distort the backbone and remove the interactions with tyrosine but should not affect prephenate binding. The addition of W259F to generate the double mutant T152P/W259F might restore tyrosine binding. Ser245 appears to play an important role in coordinating a bound water molecule which in turn likely affects prephenate binding; this will be tested by kinetic analysis of variants of Ser245. Δ19PD from *A. aeolicus* does not efficiently utilize L-arogenate as a substrate due to a very high K_m for this substrate (*50*). Comparison between the crystal structure of *A. aeolicus* Δ19PD and *Synechocystis* sp. AD indicates that Trp259 and His217 in PD are missing in the active site of AD (*41*). Therefore, removal of these two residues by H217V-W259F/Y might promote tighter binding of L-arogenate. His217 in *A. aeolicus* Δ19PD was hypothesized to be protonated to direct tyrosine's amino group away from this histidine and towards Thr152 (*41*). The pH dependence of tyrosine binding and inhibition will be conducted to determine the ionization state of His217. Modeling studies will also be performed by placing L-arogenate and prephenate within the structure that have solved at pH 7.5 in the presence of HPP and L-tyrosine. Lastly, there are no reported side-directed mutagenesis studies in AD from *Synechocystis* sp. We will commence work to help identify residues that dictate arogenate versus prephenate specificity in this TyrA protein.

References:

(1) Berg, J. M., Tymoczko, J. L., and Stryer, L. (2002) Biochemistry, p678, W. H. Freeman and Company, New York.

(2) Gibson, F., and Pittard, J. (1968) Pathways of biosynthesis of aromatic amino acids and vitamins and their control in microorganisms. *Bacteriol Rev 32*, 465-92.

(3) Coggins, J. R., Abell, C., Evans, L. B., Frederickson, M., Robinson, D. A., Roszak, A. W., and Lapthorn, A. P. (2003) Experiences with the shikimate-pathway enzymes as targets for rational drug design. *Biochem Soc Trans 31*, 548-52.

(4) Ikram Ul, H., and Ali, S. (2002) Microbiological transformation of L-tyrosine to 3, 4-dihydroxyphenyl L-alanine (L-dopa) by a mutant strain of *Aspergillus oryzae* UV-7. *Curr Microbiol 45*, 88-93.

(5) Cabrera-Valladares, N., Martinez, A., Pinero S., Lagunas-Munoz, V.H., Tinoco, R., de Anda, R., Vazquez-Duhalt, R., Bolivar, F., Gosset, G. (2006) Expression of the *melA* gene from *Rhizobium etli* CFN42 in *Escherichia coli* and characterization of the encoded tyrosinase. *Enzyme Microb Technol 38*, 772-9.

(6) Bourke, S. L., and Kohn, J. (2003) Polymers derived from the amino acid L-tyrosine: polycarbonates, polyarylates and copolymers with poly(ethylene glycol). *Adv Drug Deliv Rev 55*, 447-66.

(7) Yanofsky, C. (1988) Transcription attenuation. *J Biol Chem 263*, 609-12.

(8) Hudson, G. S., Howlett, G. J., and Davidson, B. E. (1983) The binding of tyrosine and NAD^+ to chorismate mutase/prephenate dehydrogenase from *Escherichia coli* K12 and the effects of these ligands on the activity and self-association of the enzyme. Analysis in terms of a model. *J Biol Chem 258*, 3114-20.

(9) Turnbull, J., Morrison, J. F., and Cleland, W. W. (1991) Kinetic studies on chorismate mutase-prephenate dehydrogenase from *Escherichia coli*: models for the feedback inhibition of prephenate dehydrogenase by L-tyrosine. *Biochemistry 30*, 7783-8.

(10) Chipman, D. M., and Shaanan, B. (2001) The ACT domain family. *Curr Opin Struct Biol 11*, 694-700.

(11) Ikeda, M., and Katsumata, R. (1992) Metabolic Engineering to Produce Tyrosine or Phenylalanine in a Tryptophan-Producing *Corynebacterium glutamicum* Strain. *Appl Environ Microbiol 58*, 781-5.

(12) Lutke-Eversloh, T., and Stephanopoulos, G. (2005) Feedback inhibition of chorismate mutase/prephenate dehydrogenase (TyrA) of *Escherichia coli*: generation and characterization of tyrosine-insensitive mutants. *Appl Environ Microbiol 71*, 7224-8.

(13) Lutke-Eversloh, T., and Stephanopoulos, G. (2007) L-tyrosine production by deregulated strains of *Escherichia coli*. *Appl Microbiol Biotechnol 75*, 103-10.

(14) Stenmark, S. L., Pierson, D. L., Jensen, R. A., and Glover, G. I. (1974) Blue-green bacteria synthesise L-tyrosine by the pretyrosine pathway. *Nature 247*, 290-2.

(15) Rippert, P., and Matringe, M. (2002) Purification and kinetic analysis of the two recombinant arogenate dehydrogenase isoforms of *Arabidopsis thaliana*. *Eur J Biochem 269*, 4753-61.
(16) Rippert, P., and Matringe, M. (2002) Molecular and biochemical characterization of an *Arabidopsis thaliana* arogenate dehydrogenase with two highly similar and active protein domains. *Plant Mol Biol 48*, 361-8.
(17) Hall, G. C., Flick, M. B., Gherna, R. L., and Jensen, R. A. (1982) Biochemical diversity for biosynthesis of aromatic amino acids among the cyanobacteria. *J Bacteriol 149*, 65-78.
(18) Fazel, A. M., and Jensen, R. A. (1979) Obligatory biosynthesis of L-tyrosine via the pretyrosine branchlet in coryneform bacteria. *J Bacteriol 138*, 805-15.
(19) Fazel, A. M., Bowen, J. R., and Jensen, R. A. (1980) Arogenate (pretyrosine) is an obligatory intermediate of L-tyrosine biosynthesis: confirmation in a microbial mutant. *Proc Natl Acad Sci U S A 77*, 1270-3.
(20) Bonner, C. A., Jensen, R. A., Gander, J. E., and Keyhani, N. O. (2004) A core catalytic domain of the TyrA protein family: arogenate dehydrogenase from *Synechocystis*. *Biochem J 382*, 279-91.
(21) Mayer, E., Waldner-Sander, S., Keller, B., Keller, E., and Lingens, F. (1985) Purification of arogenate dehydrogenase from Phenylobacterium immobile. *FEBS Lett 179*, 208-12.
(22) Keller, B., Keller, E., and Lingens, F. (1985) Arogenate dehydrogenase from *Streptomyces phaeochromogenes*. Purification and properties. *Biol Chem Hoppe Seyler 366*, 1063-6.
(23) Zhao, G., Xia, T., Ingram, L. O., and Jensen, R. A. (1993) An allosterically insensitive class of cyclohexadienyl dehydrogenase from *Zymomonas mobilis*. *Eur J Biochem 212*, 157-65.
(24) Patel, N., Pierson, D. L., and Jensen, R. A. (1977) Dual enzymatic routes to L-tyrosine and L-phenylalanine via pretyrosine in *Pseudomonas aeruginosa*. *J Biol Chem 252*, 5839-46.
(25) Xie, G., Bonner, C. A., and Jensen, R. A. (2000) Cyclohexadienyl dehydrogenase from *Pseudomonas stutzeri* exemplifies a widespread type of tyrosine-pathway dehydrogenase in the TyrA protein family. *Comp Biochem Physiol C Toxicol Pharmacol 125*, 65-83.
(26) Song, J., Bonner, C. A., Wolinsky, M., and Jensen, R. A. (2005) The TyrA family of aromatic-pathway dehydrogenases in phylogenetic context. *BMC Biol 3*, 13.
(27) Champney, W. S., and Jensen, R. A. (1970) The enzymology of prephenate dehydrogenase in *Bacillus subtilis*. *J Biol Chem 245*, 3763-70.
(28) Gaines, C. G., Byng, G. S., Whitaker, R. J. and Jensen, R. A. (1982) L-Tyrosine regulation and biosynthesis via arogenate dehydrogenase in suspension-cultured cells of *Nicotiana silvestris* Speg. et Comes. *Planta 156*, 233-40.
(29) Christendat, D., and Turnbull, J. L. (1996) Identification of active site residues of chorismate mutase-prephenate dehydrogenase from *Escherichia coli*. *Biochemistry 35*, 4468-79.
(30) Christendat, D., Saridakis, V. C., and Turnbull, J. L. (1998) Use of site-directed mutagenesis to identify residues specific for each reaction catalyzed by

chorismate mutase-prephenate dehydrogenase from *Escherichia coli*. *Biochemistry 37*, 15703-12.
(31) Christendat, D., and Turnbull, J. L. (1999) Identifying groups involved in the binding of prephenate to prephenate dehydrogenase from *Escherichia coli*. *Biochemistry 38*, 4782-93.
(32) Bonner, C. A., Disz, T., Hwang, K., Song, J., Vonstein, V., Overbeek, R., and Jensen, R. A. (2008) Cohesion group approach for evolutionary analysis of TyrA, a protein family with wide-ranging substrate specificities. *Microbiol Mol Biol Rev 72*, 13-53, table of contents.
(33) Legrand, P., Dumas, R., Seux, M., Rippert, P., Ravelli, R., Ferrer, J. L., and Matringe, M. (2006) Biochemical characterization and crystal structure of *Synechocystis* arogenate dehydrogenase provide insights into catalytic reaction. *Structure 14*, 767-76.
(34) Hudson, G. S., and Davidson, B. E. (1984) Nucleotide sequence and transcription of the phenylalanine and tyrosine operons of *Escherichia coli* K12. *J Mol Biol 180*, 1023-51.
(35) Turnbull, J., and Morrison, J. F. (1990) Chorismate mutase-prephenate dehydrogenase from *Escherichia coli*. 2. Evidence for two different active sites. *Biochemistry 29*, 10255-61.
(36) Christopherson, R. I., Heyde, E., and Morrison, J. F. (1983) Chorismate mutase-prephenate dehydrogenase from *Escherichia coli*: spatial relationship of the mutase and dehydrogenase sites. *Biochemistry 22*, 1650-6.
(37) Turnbull, J., Cleland, W. W., and Morrison, J. F. (1991) pH dependency of the reactions catalyzed by chorismate mutase-prephenate dehydrogenase from *Escherichia coli*. *Biochemistry 30*, 7777-82.
(38) Chen, S., Vincent, S., Wilson, D. B., and Ganem, B. (2003) Mapping of chorismate mutase and prephenate dehydrogenase domains in the *Escherichia coli* T-protein. *Eur J Biochem 270*, 757-63.
(39) Lee, A. Y., Stewart, J. D., Clardy, J., and Ganem, B. (1995) New insight into the catalytic mechanism of chorismate mutases from structural studies. *Chem Biol 2*, 195-203.
(40) Sun, W., Singh, S., Zhang, R., Turnbull, J. L., and Christendat, D. (2006) Crystal structure of prephenate dehydrogenase from *Aquifex aeolicus*. Insights into the catalytic mechanism. *J Biol Chem 281*, 12919-28.
(41) Sun, W., Shahinas, D., Bonvin. J., Hou, W., Kimber, M. S., Turnbull. J. L. and Christendat, D. (2009) in *J Biol Chem* in press.
(42) The Joint Center for Structural Genomics. (2009) Crystal structure of chorismate mutase / prephenate dehydrogenase (tyrA) (1574749) from *Haemophilus influenzae* RD at 2.00 Å resolution, PDB: 2PV7
(43) Hermes, J. D., Tipton, P. A., Fisher, M. A., O'Leary, M. H., Morrison, J. F., and Cleland, W. W. (1984) Mechanisms of enzymatic and acid-catalyzed decarboxylations of prephenate. *Biochemistry 23*, 6263-75.
(44) Sampathkumar, P., and Morrison, J. F. (1982) Chorismate mutase-prephenate dehydrogenase from *Escherichia coli*. Kinetic mechanism of the prephenate dehydrogenase reaction. *Biochim Biophys Acta 702*, 212-9.

(45) Christopherson, R. I., and Morrison, J. F. (1985) Chorismate mutase-prephenate dehydrogenase from *Escherichia coli*: positive cooperativity with substrates and inhibitors. *Biochemistry 24*, 1116-21.
(46) DeLano, W. L. (2002) in *The PyMOL Molecular Graphics System*, San Carlos, CA.
(47) Kawasumi, T., Igarashi, Y., Kodama, T., and Minoda, Y. (1984) *Hydrogenobacter thermophilus* gen. nov., sp. nov., an extremely thermophilic, aerobic, hydrogen-oxidizing bacterium. *Int J Syst Bacteriol 34*, 5-10.
(48) Huber, R., Wilharm, T., Huber, D., Trincone, A., Burggraf, S., Ko¨nig, H., Rachel, R., Rockinger, I., Fricke, H., and Stetter, K.O. (1992) *Aquifex pyrophilus* gen. nov., sp. nov., represents a novel group of marine hyperthermophilic hydrogen-oxidizing bacteria. *Syst Appl Microbiol 15*, 340-51.
(49) Deckert, G., Warren, P. V., Gaasterland, T., Young, W. G., Lenox, A. L., Graham, D. E., Overbeek, R., Snead, M. A., Keller, M., Aujay, M., Huber, R., Feldman, R. A., Short, J. M., Olsen, G. J., and Swanson, R. V. (1998) The complete genome of the hyperthermophilic bacterium *Aquifex aeolicus*. *Nature 392*, 353-8.
(50) Bonvin, J., Aponte, R. A., Marcantonio, M., Singh, S., Christendat, D., and Turnbull, J. L. (2006) Biochemical characterization of prephenate dehydrogenase from the hyperthermophilic bacterium *Aquifex aeolicus*. *Protein Sci 15*, 1417-32.
(51) Bonvin, J. (2008) PhD thsis, Department of Chemistry and Biochemistry, Concordia University, Montreal, CA.
(52) Dudzinski, P. K., Morrison, J. F. (1976) The Preparation and Purification of Sodium Prephenate. *Prep Biochem 6*, 113-21.
(53) Rieger, C. E., and Turnbull, J. L. (1996) Small scale biosynthesis and purification of gram quantities of chorismic acid. *Prep Biochem Biotechnol 26*, 67-76.
(54) Dawson, C. M. R., Elliott, C. D., Elliot, H. W. and Jones, M. K. (1986) *Data for Biochemical Research*, 3rd edition ed., Oxford Science Publications, Clarendon Press.
(55) Turnbull, J. L. (1988), PhD thesis, Australian National University, Canberra, AU.
(56) Sambrook, J., Russell, D. (2001) *Molecular Cloning*, 3rd ed., Cold Spring Harbor Laboratory Press, Cold Spring, New York.
(57) Rozen, S., Skaletsky, H.J. (2000) Primer3 on the WWW for general users and for biologist programmers, in *Bioinformatics Methods and Protocols: Methods in Molecular Biology* pp 365-386, Humana Press, Totowa, NJ.
(58) NCCLS Approved Standard ACS-1 (1979) *Specification for Standardized Protein Solution (Bovine Serum Albumin)*, 2nd ed., National Committee for Clinical Laboratory Standards: Villanova, PA.
(59) Weinglass, A. B., Whitelegge, J. P., Hu, Y., Verner, G. E., Faull, K. F., and Kaback, H. R. (2003) Elucidation of substrate binding interactions in a membrane transport protein by mass spectrometry. *EMBO J 22*, 1467-77.
(60) Schmid, F. X. (1998) *Spectral methods of characterizing protein conformation and conformational changes*, TE Creighton edition IRL press, Oxford, UK.
(61) Aponte, A. R. (2002) M.Sc. thesis, Department of Chemistry and Biochemistry, Concordia University, Montreal, CA.